sustainability

MDPI

Article

Soft-Switching Smart Transformer Design and Application for Photovoltaic Integrated Smart City Power Distribution

Burak Esenboğa * and Tuğçe Demirdelen

Department of Electrical Electronics Engineering, Adana Alparslan Türkeş Science and Technology University, Sarıçam 01330, Adana, Turkey

* Correspondence: besenboga@atu.edu.tr

Abstract: Smart city power distributions have become promising technologies to meet the demand for energy in developed countries. However, increase in smart grids causes several power quality problems on the smart grid, in particular, current and voltage harmonic distortions, sudden voltage sag and swells, fault current, and isolation deterioration. Smart transformers are potential solutions to improve the power quality on the electric grid. They present energy efficiency, ensure grid reliability and power flow control, voltage regulation, bidirectional power flow, fault current limiting, harmonic blocking, and galvanic isolation. Therefore, this paper offers an optimal selection of a three-stage (AC-DC-DC-AC) smart transformer model and power control strategy for solar PV power plant integrated smart grids. The topology of the rectifier, isolated bidirectional converter, and inverter has soft-switching features. This enables low conduction loss, low electromagnetic interference (EMI), high efficiency, achievable zero-voltage switching for converters, and zero-current switching for electrical auxiliary systems. Operation strategies of the proposed ST, PWM control, voltage, and current control between converters, including a medium-voltage (MV) high-frequency transformer to realize a 10 kVA, 450 Vdc to 220 Vdc, or 220 Vac ST, are presented. Significantly, the ST prototype achieves 96.7% conversion efficiency thanks to its control strategy, even under unstable power generation conditions from the solar PV plant. Experimental results obtained on the 344 Vac 10.4 A load current validates the dv/dt rate 6.8 kV/us. The dynamic and experimental results of the proposed bidirectional smart transformer demonstrate the success in preventing power quality problems for photovoltaic integrated smart city power distribution.

Keywords: smart transformer; power quality; smart city; power distribution; solar PV

Citation: Esenboğa, B.; Demirdelen, T. Soft-Switching Smart Transformer Design and Application for Photovoltaic Integrated Smart City Power Distribution. *Sustainability* **2023**, *15*, 32. https://doi.org/10.3390/su15010032

Academic Editors: Surender Reddy Salkuti and Brian Azzopardi

Received: 31 October 2022
Revised: 2 December 2022
Accepted: 9 December 2022
Published: 20 December 2022

1. Introduction

In recent years, the increasing use of renewable energies and distributed generation bring about energy quality problems in the smart power grid. Smart transformers (STs) are key and intelligent technologies that allow the incorporation of renewable and non-renewable power plants into the same electric grid. STs have many advantages that are becoming an alternative to substitute the conventional power transformer such as reactive power compensation, voltage regulation, power flow control, bidirectional power flow, fault current limiting, harmonic blocking, and galvanic isolation. One of the most significant features of STs is that the weight and size are reduced considerably compared with the conventional power transformers. This advantage is gained with the dc–dc isolated converter structure of the ST. The dc–dc conversion stage with HF transformer is the main part of the ST since it achieves some requirements such as high efficiency, high power density, intelligent power flow management, better isolation, reduced size, and weight. In smart grids, it is the main part where power is controlled, and grid reliability is ensured. To meet these significant requirements in the different application areas of STs, researchers have performed many studies on STs integrated smart grids. The literature review presents the dc–dc converter-based ST studies so far. The literature review is summarized in Table S1.

A three-stage modular multilevel converter-based ST is presented [1–7]. This converter provides bidirectional power flow due to its dual active structure. The control method of the ISOP converter is the open-loop control (OLC) method. The study shows that the proposed converter structure meets the requirements for isolation [1]. To increase the power range, reduce the voltage harmonics, reduce the dv/dt stress and eliminate the back power flow, the modular multilevel converter is proposed. The voltage regulation and current balance operation are provided by the dual shift control method [2]. The modular multilevel converter (MMC) has a high conversion ratio, zero current switching operation, variable conversion ratio, and phase shift control. The faults are easily bypassed due to their modular structure. Also, the resonant operation mode eases the ZCS mode. The inductorless structure of the proposed converter provides low cost and high efficiency [3]. This converter topology is preferred to increase the converter power rating and gain high efficiency under the ZVS operation of the power switches. PI controller-based phase shift modulation is used for the control scheme. The control method enables the voltage balance of the converter [4]. An isolated bi-directional dc–dc converter in an ISOP modular topology is used in the design of a 100 kVA ST-based power substation to reduce the freewheeling currents of DAB, which raise overall losses and lower the effective duty cycle. To demonstrate the effectiveness of the suggested approach, simulation results in the Matlab-Simulink environment are shown. For tracking a sinusoidal reference signal, a proportional resonant (PR) controller performs better than a PI controller. However, due to its limited bandwidth, a conventional PR controller is difficult to make stable. An updated PR controller is incorporated into the design to address this issue. The developed controller is stable and functions well thanks to the low steady-state error and reliable output [5]. The Quasi-2-Level (Q2L) modulation strategy is proposed for the control of the system due to its effectiveness and superior current transfer capacity. Also, the proposed control method provides to suppress the dv/dt on the HF transformer. The results show that the Q2L modulation strategy achieves the capacitor voltage balance and lower electromagnetic interference (EMI) [6].

A series resonant converter is proposed [8–18]. This converter topology is used to meet the constant voltage-transfer requirement of the phase modular STs. The half-cycle discontinuous conduction-mode operation principle is selected for the isolation stage of the ST since this operation achieves zero current switching with high efficiency. However, the operating strategy lacks power flow control. This operation mode provides to circulate the MV side power fluctuations through the SRC to the common LV side [10]. A new single-stage control method is used to simplify the system control. This converter has a quasi-resonant frequency mode, because the constant voltage is obtained for the common DC-side voltage thanks to this model [8]. The conventional series resonant converter is reconfigured to provide voltage stability by using a voltage doubler rectifier. The proposed converter structure achieves the post-fault operation and decreased additional power devices [12]. A CLLC resonant converter is used for a next-generation DC data center. The proposed converter provides ZVS operation of the primary power switches. To minimize the power flow losses, synchronize rectifier control is used for output side power switches. Also, the switching frequency and resonant frequency operate simultaneously to get better conversion efficiency. The results show that the designed converter topology achieves 98% peak efficiency and good power density [14]. The resonant soft-switching modulation is applied for the control technique of the proposed dc–dc converter. The control method increases the system's efficiency because of its soft switch loss reduction capability [18].

A dual active bridge (DAB) converter is proposed for the MV dc–dc isolation stage of the STs [19–47]. This converter has many superiorities such as zero-voltage switching (ZVS), simple control, high power isolation, and bidirectional power flow. Yet, the parasitic capacitances are especially high at high frequency and voltage levels. This case results in the switching losses and slowing of dV/dt [19]. Contrary to conventional single-phase shift control, the extended phase shift control method is applied to minimize power losses. The proposed control strategy manages to adjust the direction and magnitude of power

flow. The backflow power is reduced by extended phase shift control [30]. The phase angle control method is only applied for the DAB voltage control due to its simple and easy implementation capability. Also, the HF transformer is chosen as a star-delta connection to reduce the turn ratio. The smaller and closer turns of the HF transformer enable the ZVS operation [40]. To reduce the harmonics and inrush current effects, the soft-shift modulation control is offered for the isolation stage of the ST. The proposed control method provides the voltage balance and regulates the dc-link capacitor voltages of the dc–dc converter [44].

A power electronic-based intelligent universal transformer is proposed for the utility grid. The isolation stage of the proposed smart transformer is an LLC based converter to provide soft-switching operation. To manage the voltage and power flow, a DSP based control card is used. The proposed converter allows the low magnetizing current thanks to their leakage inductances. The converter provides 98% maximum efficiency under light load conditions [46]. A medium frequency isolated transformer structure is presented for a 500 kVA industrial prototype electronic power transformer. The isolation stage consists of cascaded voltage source converters and medium-frequency transformers. The pulse width modulation control, current and voltage inner loop control structure are used in a DSP to control the unbalanced output power. The fault protection and monitoring operation are also achieved thanks to DSP [47].

A Quadruple-Active-Bridge (QAB) dc–dc converter is examined for a modular ST configuration [48–50]. This converter topology is selected for soft-switching capability and reduction in the number of high-frequency transformers. Triangular current modulation is used to control the converter. This control strategy uses the duty cycle principle to control the power switches. It provides to reduce the circulating reactive power in the isolation stage of ST [48]. This converter type is used to reduce the number of HF transformers to provide more bridges for the connection of HF transformers. The triangular current-mode modulation control is applied to achieve the soft-switching operation of the power switch. The control strategy enables it to reduce the power switching losses and ease the ZCS operation for heavy loads [49].

The literature review presents the STs used in smart power grids. The studies reveal that dual active bridge converters, resonant converters, modular multilevel converters, and quadruple active bridge converters are widely used in ST applications. The four main dc–dc conversion structures in different applications and powers are presented with their control strategies. Related to this study, ST models for solar PV power systems are presented in References [51–56]. To reduce the dual-side backflow power and increase the DAB converter's effectiveness for a variety of voltage conversion situations, a single-stage dc smart transformer based on a DAB converter is developed. Enhanced triple-phase shift control and single-phase shift control methods are applied to the DAB converter to show the effectiveness of the proposed enhanced triple-phase shift control. The efficiency of the DAB converter-based ST model is measured at 96% thanks to the proposed control algorithm [51]. For MV-level grid-tied applications, such as power converters for renewable energy systems and electric trains, single-stage loosely coupled resonant DAB converter-based ST is used. Loosely coupled coils are used in place of the HF transformers used in traditional STs. The efficiencies of the proposed DAB converter and ST model are 97.4% and 95.2% at 2.4 kW [52]. A forward dual-active-bridge-based ST topology is presented. This topology decreases the number of active switches, and it is aimed at further reduction in the converter volume. The proposed topology is demonstrated to be superior to other unidirectional topologies in three areas: higher power density with commercially available power modules, lower part count, and ease of control [53]. The reactive power distribution method is proposed for a cascaded multilevel converters-based ST topology. Due to the increasing reactive power in solar cells, it is anticipated that the efficiency of such power cells will decline as the imbalance rises. This method involves allowing some power cells to carry a higher AC for a given active power than they would under balanced conditions. It lessens unbalanced power on the solar cells [54]. The simulation model and management of a three-stage ST with a solar PV power plant are presented. For the conversion of various

stages, a PWM rectifier, a DAB, and a three-phase voltage source control inverter are used. Changes in solar irradiation, load demand, and irregularities in grid supply voltages have all been found to affect ST. Under a variety of field disturbances, the performance of ST has been deemed adequate [55]. A DAB converter-based ST model for solar PV systems is created in MATLAB/Simpower, and a prototype is implemented in the laboratory. The proposed ST can efficiently integrate solar PV modules into the grid/load, according to simulation and experimental results, with the LCL filter demonstrating a good reduction of undesirable harmonics. The ST with a dual active bridge increases efficiency and power transfer based on the relative phase shift between each h-bridge switching [56]. In this study, the cascade (AC–DC–DC–AC) soft-switching smart transformer model is used for the first time for a real smart power grid. The proposed DAB converter-based ST model is implemented in a real-time 12.5 kW solar PV power plant. Under partial shading conditions, the output power obtained from solar PV panels is constantly changing. This causes large power imbalances in the smart grid. Soft-switching features of the proposed ST will provide low conduction loss, low electromagnetic interference (EMI) for the converters and high efficiency, and balanced power for the end-users. With the proposed control method and key driving strategies in converters, DAB converter and ST conversion efficiency is aimed at over 98% and 96%, respectively. The proposed ST topology and easy-to-apply control method are tested on a real solar PV power plant. The ability of the smart transformer to control power against sudden power changes in solar PV plants has been verified with ZVS gain, dv/dt ratio, and conversion efficiency. Also, the proposed system can be connected to both ac and dc sources or loads thanks to bidirectional power flow. Additionally, the proposed control algorithm of the ST is easy applicable and multifunctional to solve the power sag and swell problems. Therefore, soft switching ST enables power control and efficient use of electrical energy in a grid struggling with unwanted power flow from interconnected grids such as grid-connected renewable power plants.

This paper is presented in 3 sections. All dc–dc converter structures used in different ST applications are reviewed in the introduction section. In the literature review, the converter topologies are evaluated in terms of switching characteristics, application areas, frequency, isolation level, and ZVS and ZSC operations. Materials and methods consist of soft switching medium voltage dc smart transformer topology, operation principle of DAB converter, control schemes, and solar PV power plant, presented in Section 2. In Section 3, a solar PV power plant-based ST dynamic model is created in MATLAB/Simulink to show the performance analysis of the proposed photovoltaic integrated smart city power distribution. The design and control application of the proposed ST model is examined in detail. Finally, the inferences obtained from the simulation and experimental results, and the proposed ST success are explained in the conclusion section.

2. Materials and Methods

2.1. Soft Switching Medium Voltage dc Smart Transformer Topology

The schematic of the proposed soft switching MVdc ST with a control strategy to interface MVdc or low voltage ac (LVac) loads or sources with smart grids is shown in Figure 1. The dc–dc converter module is based on the soft-switching smart transformer topology with reduced conduction loss thanks to their voltage, current, and PWM control strategy. The dc–dc converter module is formed by two reverse-blocking semiconductor bridges, a high-frequency transformer to provide galvanic isolation, and auxiliary resonant circuits to create ZVS conditions for all the major components.

The dc–dc conversion stage is the key part for three-level STs since the whole power system efficiency generally depends on the dc–dc conversion efficiency. The high-frequency isolated dc–dc converters are significant devices for future smart-grid applications due to their acts as a DC transformers. However, the most challenging and remarkable stage is the dc–dc conversion stage of the ST because it must meet some strict requirements to achieve high conversion efficiency and galvanic isolation. These requirements are exemplified as a fast-switching speed, ZVS, ZCS, zero load current, minimum hard turn-on loss, low di/dt

feature, high-frequency isolation, high-rated power, soft switching, and power density. While providing some requirements, researchers used variable converter topologies in different applications.

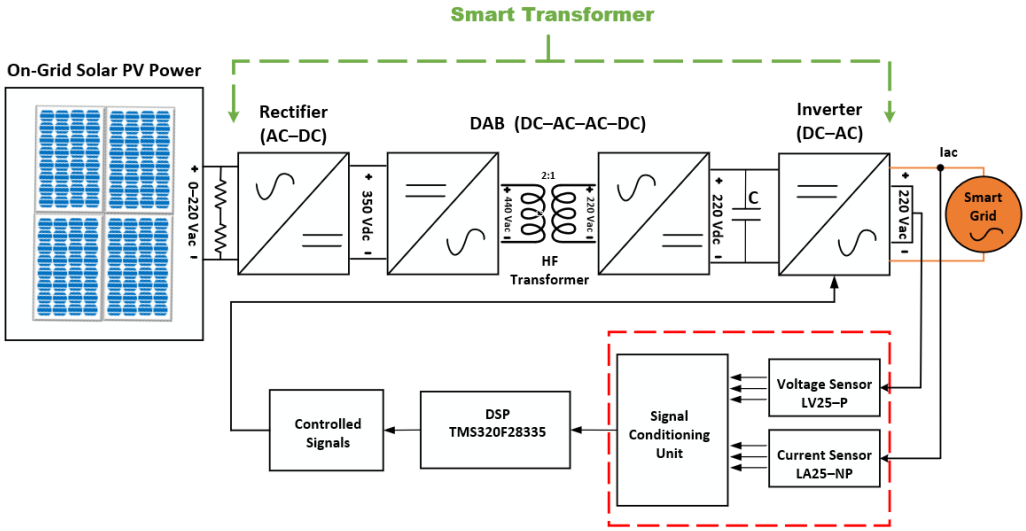

Figure 1. The proposed smart transformer topology for the smart city power grid.

The isolated dual active bridge converters are widely used in many applications to achieve bidirectional power flow and ZVS operation. Thus, the switching losses are reduced thanks to ZVS operation for high efficiency and high power density. This feature allows the use of DAB converters in DC microgrid applications and battery management systems. However, these converters are exposed to the high circulating current at higher loads and ZVS fails at light loads. The switching losses occur under the light load. The harmonics arise from the high dv/dt, light load, and electromagnetic interference in the HF transformer. Therefore, HF transformer design and the selection of the power switches play a significant role in the conversion efficiency of the converter. The isolated DAB dc–dc converter for the STs is given in Figure 2. Also, Table 1 presents the comparative analysis of the dc–dc converters used in STs.

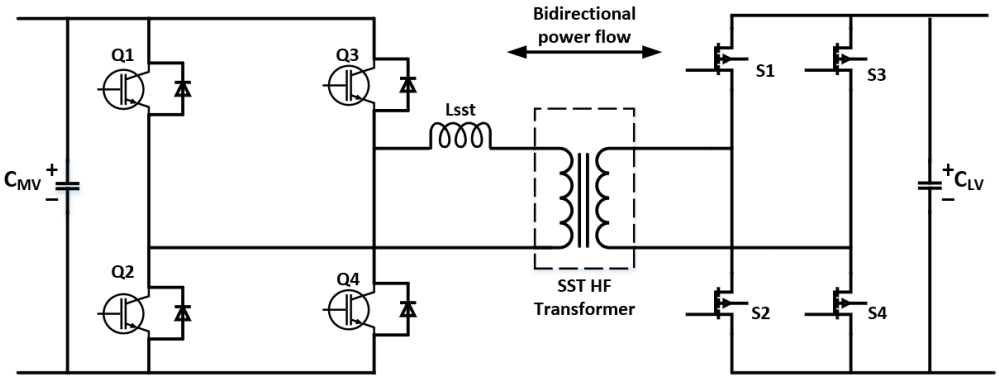

Figure 2. Isolated dual active bridge converter topology for smart transformer.

The proposed dual active bridge (DAB) dc–dc converter consists of the HF transformer and two h bridge bridges of medium voltage and low voltage. The DAB converter with 10 kVA power has a voltage reduction feature from 800 Vdc to 400 Vdc. The HF transformer is used at a power of 10 kVA according to the switching frequency of 20 kHz. Phase-shifted duty square waves, voltage, and current control techniques are used to control the power flow. The proposed DAB converter uses two inductors. These are the magnetizing inductance and the primary leakage inductance. While reducing current harmonics and

preventing unexpected voltage spikes, and leakage inductance, the high-frequency transformer's circulating current causes electromagnetic interferences, which are lessened by the magnetizing inductance. As a result, the HF transformer and power switches' power losses are reduced, and the converter's efficiency is raised. The DAB converter can be used in smart grids because it can provide bidirectional power flow, and interface the LVdc grid or the LVac grid. Also, it can achieve higher efficiency by providing ZVS control with the best control strategy. Thus, the proposed dc–dc converter module can feature a single-stage high-frequency link power conversion architecture, reduced dv/dt, full-range ZVS, and robustness with benign fault modes such as short circuit current limiting from the dc-link inductor, desaturation protection in gate drivers, and limit parasitic-inductance-induced voltage spikes.

Table 1. The comparative performance analysis of the dc–dc converters used for STs.

Converter	dv/dt at Turn-on of the Main Switch	Resonant Circuit Connection	Bidirectional Power Flow Speed	Circulating Current	Soft-Switching Range	Multiple DC Cable Connections
MC	<10 kv/us	Resonant Tank	>1 us	High	>100 ns, <600 ns	practicable
SRC	>10 kv/us, <100 kv/us	Series Resonant Tank	<1 us	Medium	>100 ns, <100 us	impracticable
DAB	<10 kv/us	LLC Resonant Tank	<1 us	Low	>100 ns, <100 us	practicable
QAB	<10 kv/us	No	>1 us	High	>100 ns, <600 ns	practicable

2.2. Operation Principle

Isolated bidirectional DAB converters consist of two full bridge circuits and an HF transformer as shown in Figure 1. The leakage inductance of the high-frequency transformer is presented. The voltage gain conversion ratio of DAB is:

$$d = \frac{aC_{MV}}{C_{LV}} \tag{1}$$

fs is given as the switching frequency, φ is a phase shift between the two bridge circuits, L_{sst} is the leakage inductance of the MV side bridge circuit, and T_{hs} is half of the switching period. The transmission power given between two h-bridge circuits is:

$$P_T = \frac{aC_{MV}C_{LV}}{w_s L_{sst}}\varphi\left(1 - \frac{\varphi}{\pi}\right) \tag{2}$$

Also, leakage inductance currents of two bridge circuits are given as I_{sst1} and I_{sst2}.

$$I_{sst1} = -\frac{T_{hs}C_{MV}}{2\pi L_{sst}}(2d\varphi + \pi(1 - \mathrm{d})) \tag{3}$$

$$I_{sst2} = \frac{T_{hs}C_{MV}}{2\pi L_{sst}}(2\varphi + \pi(\mathrm{d} - 1)) \tag{4}$$

These currents determine the switch-on losses of the circuits. To achieve the zero-voltage switching of two bridges, the states are $I_{sst1} < 0$ and $I_{sst2} > 0$, respectively. In this situation, the body diode of the switch that needs to be turned on receives the current from the leakage inductance. Additionally, the DAB converter ensures deadband to protect the dependability of the high voltage and high power converters. In order to determine how much of the leakage inductance's current is necessary for the ZVS turn-on operation at the start of the deadband, it is critical to study the converter at this point. Figure 3 shows the key waveforms of the DAB during deadband ([t0 t2]). Figure 4 shows the equivalent circuits of the DAB converter, which include the current path in various modes during deadband.

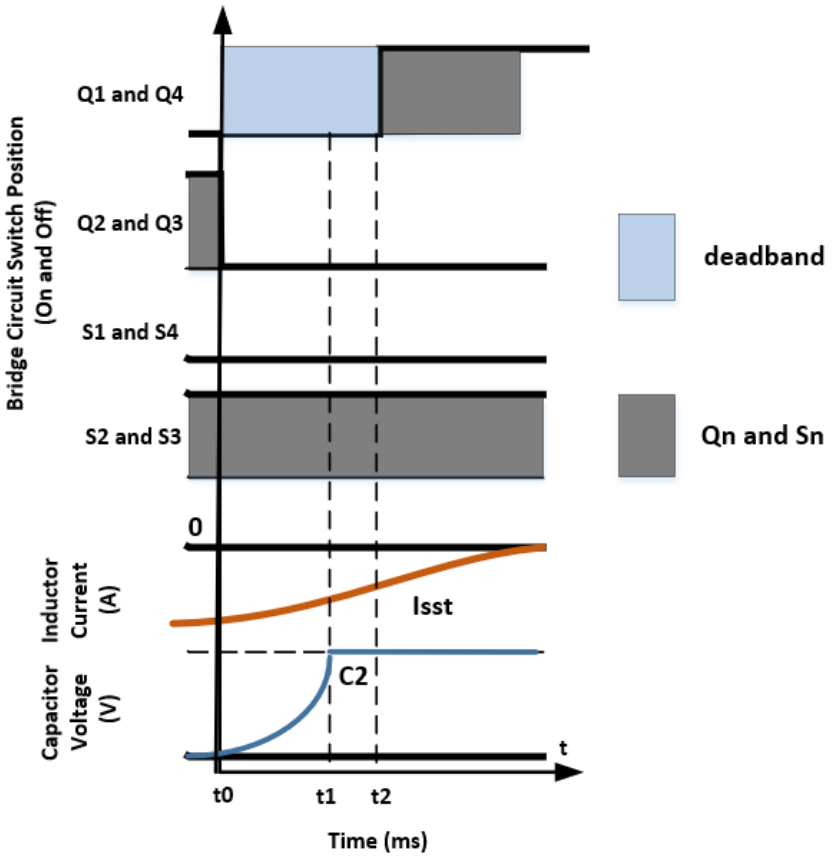

Figure 3. The voltage of the ZVS capacitor of C2 under deadband, the leakage inductance current I_{sst}, and the PWM gate signals of power switches.

2.3. Control Scheme

The control strategies of the converters have a direct effect on the performance of the STs. The variable control systems are applied for converters in the literature survey. The voltage and current control method is used to provide voltage balance and output current sharing in the ST. The voltage and current balance are significant operations to protect the power switches from burnout. The dc voltage balance prevents the early failure of some IGBT devices. Similarly, the current sharing control is an effective control strategy to reduce the switching losses and heat stress on the power switches. Thus, the voltage and current control strategy enable the avoidance of risks of overcurrent and overvoltage in the power electronic system.

Frequency control is generally used in the series resonant converter-based STs. Due to keeping the switching frequency close to the resonant frequency, power switches can succeed in zero-voltage switching and zero-current switching. This case results in little switching losses on the power switches. Also, the trapezoidal modulation can minimize the turn-off losses of the power switches because the switch-off operation is achieved under the ZVS. Discontinuous conduction mode operation is also used in series resonant converter-based STs. This mode operates in the manner that the switching frequency is close to the resonance frequency in the converter. This control method achieves the ZVS operation at the MV side and the ZCS operation at the LV side. It reduces the electromagnetic interference on the HF transformer due to its low di/dt capability. The Quasi-2-Level control strategy enables the active power transfer capability. The Q2L control mechanism is based on the capacitor voltage balance strategy. It protects the HF transformer from electromagnetic interferences, reducing the dv/dt stress on the MF transformer.

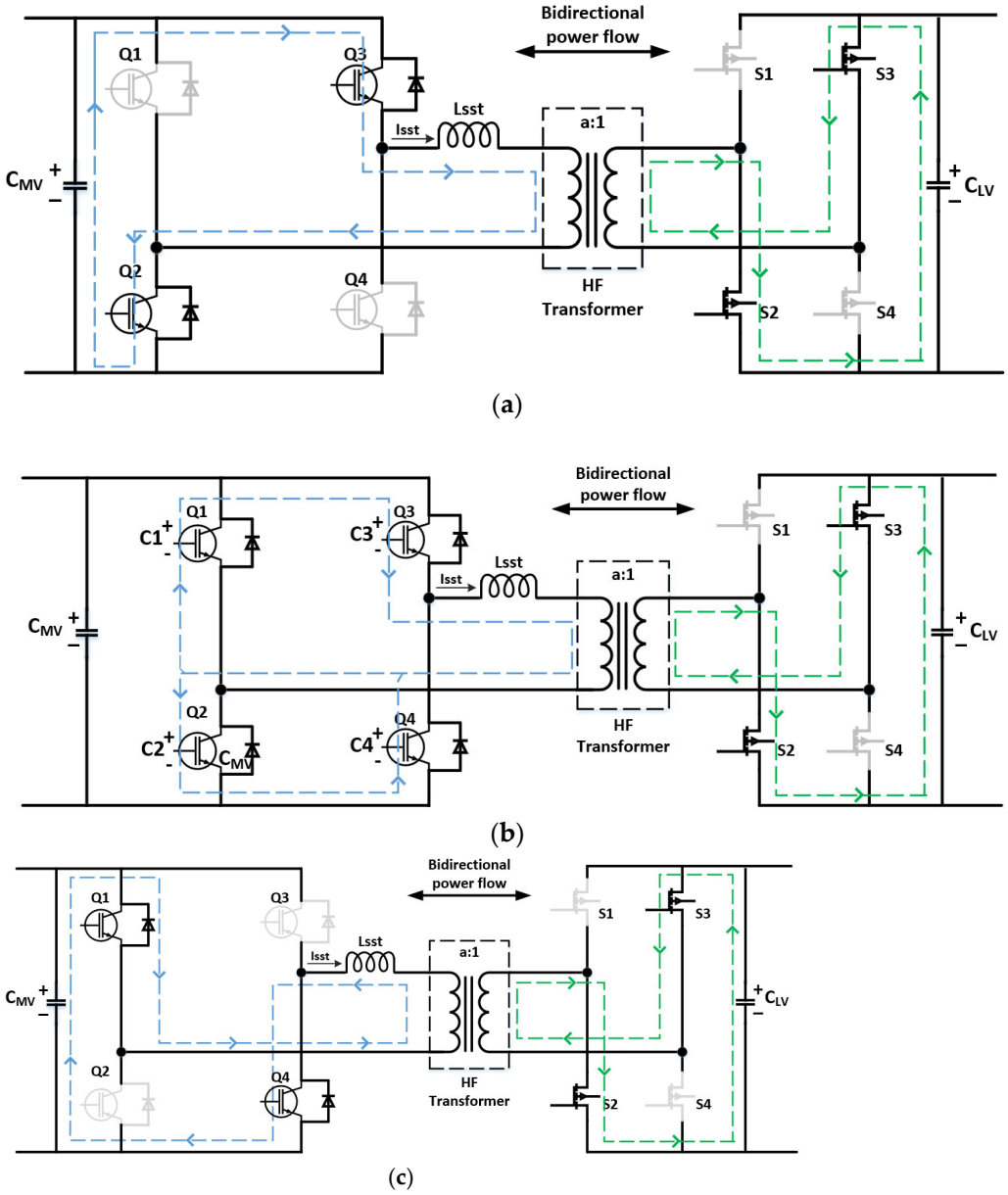

Figure 4. DAB converter including current path in different modes during deadband: (**a**) mode 0 ([t < t0]), (**b**) mode 1 ([t0 t1]), (**c**) mode 2 ([t1 t2]).

Duty cycle control has a significant role in the power conversion efficiency of the ST. Considering the MV and LV side harmonic conditions, the duty cycles are adjusted to enable a wide ZVS range, minimum circulating current flow, and power switching loss reduction. Triangular current modulation is a great solution to obtain the wide soft-switching range under the unstable output capacitor voltage terms. This control strategy manages the duty cycle to control and prevent the circulating reactive power. However, compared to the conventional phase-shift modulation, the currents' high root-mean-square (RMS) value on the power switches and HF transformer lead to higher conduction losses due to its triangular shape. The D-Q control can provide ZVS operation of the dc–dc converter by adjusting the duty ratio. The LV side voltage of the converter is controlled while the D-axis current operates freelance with the Q-axis current by arranging the duty ratio. This case gains the fast response of the power switches and overcurrent protection.

Phase shift modulation can control the power flow and cope with overcurrent problems. It allows the ZVS operation to turn on by changing the phase shift between the bridges. Nevertheless, to avoid the sudden phase shift in the dc–dc converter, an additional

control mechanism is necessary for minimizing the peak current. The OLC method is proposed in such a quick phase-shifted case. The increasing phase shift angle is controlled with proportionality to the time step, so the LV side voltage of the dc–dc converter is regulated. The commonly used control for all dc–dc converters is the pulse width modulation strategy. PWM signals are applied to control the power switches. The pulse width modulated signals operate with a 50% duty ratio. The two square wave phase-shifted signals control the turn-on and turn-off operation of the power switches, so the power flow is regulated. MV-side and LV-side capacitor voltages of the dc–dc converters should be adjusted according to the charging and discharging time by using the PWM technique. Controlling the turn-on and off times of the power switches and input/output voltages with PWM can reduce the circulating current and minimize the losses in STs.

To summarize all the implications, phase shift modulation techniques are the most widely used in terms of ease of application and control capability. However, the phase shift modulation strategy is applied to control the switches, but this control method is suitable for steady-state conditions. Therefore, additional control algorithm methods are used for the overcurrent, overvoltage, and soft-switching operation. These are the extended phase shift control method, PI controller-based single phase shift control method, and output voltage or current control methods. The additional control algorithms are used for a grid-connected solar photovoltaic (PV) system. They achieve the current and voltage balance control of converters. In this study, the PWM signals of inverter module are controlled by using a DSP control card and the Matlab/Simulink program. The output voltage is measured by a LV25-P sensor and current is measured by a LA25-NP sensor. These signals are read and scaled with the Simulink blocks and PWM controls are provided to obtain reliable output signals as shown in Figure 5. Also, the duty cycle control of the DAB is presented in Figure 6.

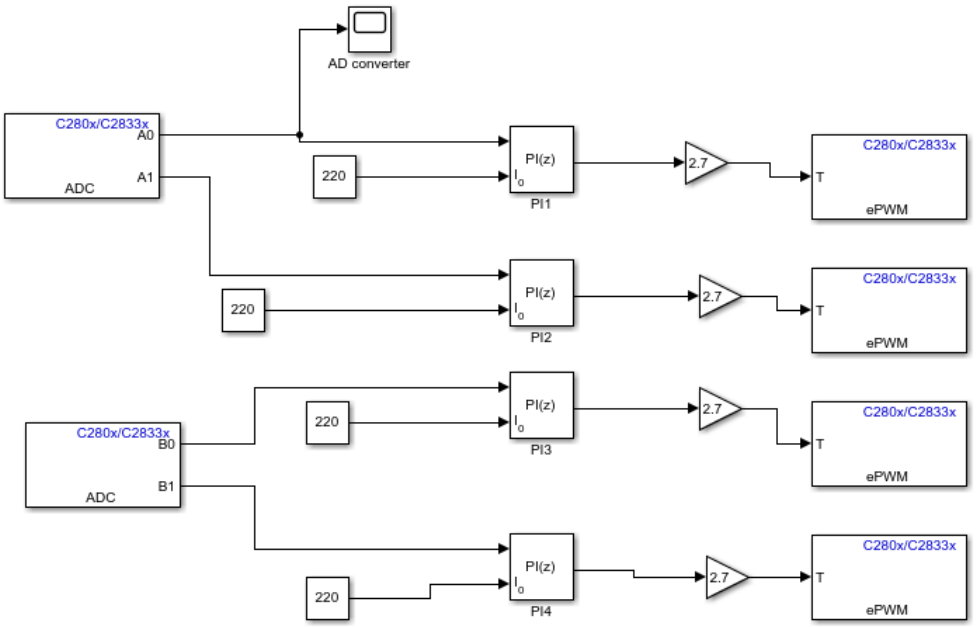

Figure 5. DSP PWM control model for inverter output voltage.

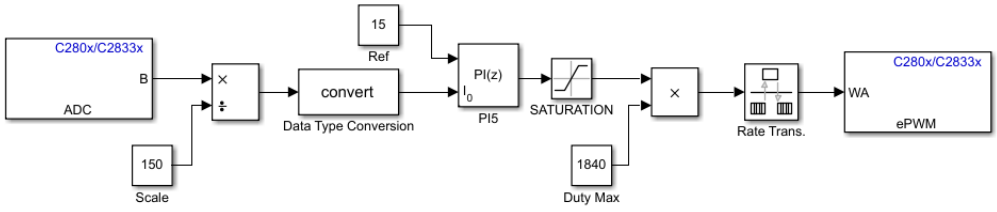

Figure 6. Duty cycle control of DAB.

To obtain voltage information from the single-phase power system, a LEM LV 25-P voltage sensor with a single-phase error conversion ratio of 220/5 volts and a supply voltage of +15 and −15 is connected. Voltage information is read from the output of the voltage sensor and directed to the zero-crossing detector. The circuit diagram of the voltage sensor connected in parallel to the circuit is shown in Figure S1.

Rm measures the resistance, while Ri represents the major input resistance. The observed power supply voltage for this study was a single-phase 220 V system operating at a 50 Hz line frequency. The analog-to-digital (ADC) range used by the DSP TMS320F28335 must match the output waveform specified by this converter. The conversion ratio for this LV 25-P voltage converter is 2500:1000, according to the voltage converter's data sheet [57]. Reducing the input voltage level from 220 V to 5 V is the primary goal. By applying Ohm's Law and using the primary rated RMS current of 10 mA, resistors are determined. The secondary side of the voltage converter's design is maintained. The secondary output current is pulled at 25 mA when the input current is 10mA according to the conversion ratio in the datasheet, which is 2500:1000. As a result, using Ohm's Law, Rm is the measurement resistance and Ri is equal to 22 k. As a result, the system voltage level, which in the circuit diagram is 220 V, is changed to 5 V at AC RMS value.

According to the design requirements, the current sensor must transform an input current into a proportionate voltage value. In this investigation, the current transducer LA 25-NP is used. Figure S2 illustrates the preferred LA 25-NP connection in detail. Voltage and current transducers make up the single-phase power measurement board. Using a conversion circuit, the measured voltage values for both transducers must be rescaled to match the ADC voltage level in the specified DSP.

Because the DSP accepts the 0–3 V input data range, low-level bipolar voltage signals in the ±5 V range are now converted to the 0–3 V range. The circuit detail for the above signal conversion requirement is shown in Figure S3.

2.4. Solar PV Power Plant

Grid-connected (on-grid) solar systems are established to operate based on the electricity produced by solar panels, where it is instantly consumed from storage, where it is produced, and the surplus is given to the grid. With the increase in the installation of such solar PV systems, energy management and efficiency in power grids have become important. In this study, a 12.5 kWp on-grid solar PV power plant was used for smart transformer input power. This solar PV power system is shown in Figure 7. The solar PV power plant consists of 30 units of 415 W solar PV panels and 6 units of 2 kW on-grid inverter modules. The solar PV power plant is mounted on the roof to meet the needs of a house. There are instantaneous voltage changes according to variable weather conditions. Experimental studies of the proposed smart transformer have been carried out on this power plant to ensure the stability of the smart grid.

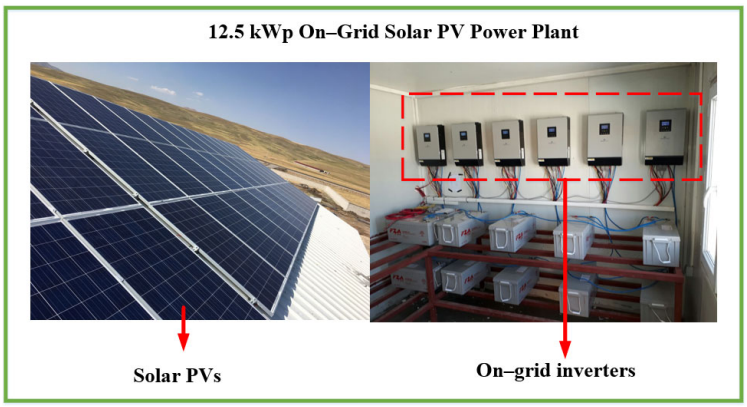

Figure 7. 12.5 kWp on-grid solar PV power plant.

3. Dynamic and Experimental Model of Smart Transformer for Smart Grids

3.1. Dynamic Model

In this paper, it is decided to analyze the impedance and efficiency characteristics of the bidirectional dc–dc dual active bridge (DAB) converter-based ST. To increase the grid reliability and power stability of a solar-powered smart grid, the performance analysis for a smart grid is proposed using a DAB-based ST. Figure 8 presents on-grid solar PV power plant-based ST. The DAB converter is not only used in the ST to enable the DC micro-grid but also serves as a power electronics interface for battery modules, other sources, or loads due to its bidirectional power flow capability, zero voltage switching (ZVS) ability, and galvanic isolation. Zero Voltage Switching is one method that enables a return to greater switching frequencies with increased input voltage and voltage drop (ZVS). This method uses pulse width modulation (PWM)-based operation, like almost all other modern switching voltage regulators, but with an additional independent phase to the PWM timing to support ZVS operation. ZVS offers soft switching, preventing the switching losses that are often experienced during traditional PWM operation and timing. While ZVS runs on a constant off-time control, zero current switching (ZCS) runs on a constant on-time control. When output voltage control or power flow control is required, the DAB converter is more advantageous because it works with active control of the transferred power. Also, under normal load conditions, this isolated converter operates at the resonant point to achieve zero voltage (ZVS) turn-on at the primary side and zero current (ZCS) turn-off at the secondary side.

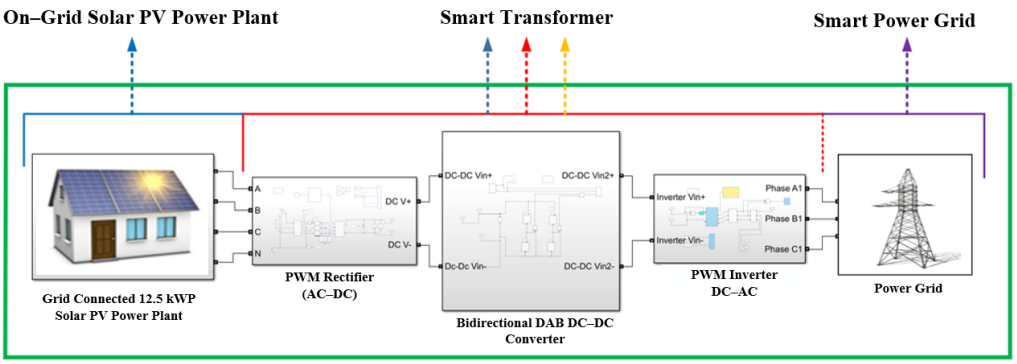

Figure 8. The model of DAB converter-based ST for a smart grid.

Figure 9 shows the proposed solar PV power plant model. 12.5 kW grid-connected solar PV power plant is modeled to provide renewable power for a smart grid. Because the average electricity consumption of a house is approximately 10 kW of power per month, the 'Perturb and Observe' technique is used in the MPPT charge controller. The solar PV panel voltage and current are measured, and instantaneous power is calculated using these two values. Then, the output power change is observed by changing the solar PV panel operating voltage. If the output power is increased, it is understood that the direction of change of the voltage is correct and by continuing in this direction, the maximum power point is obtained thanks to the proposed method. This method is proposed to improve power tracking accuracy and dynamic performance in rapidly changing environmental conditions.

In Figure S4, the solar PV panel output power and the load side output power are calculated and compared using current and voltage values. Then, the voltages are compared. Hereafter, the reference value (voltage) is increased or decreased by the specified amount. When it reaches the maximum power point, it will constantly perturb and observe operation at that point.

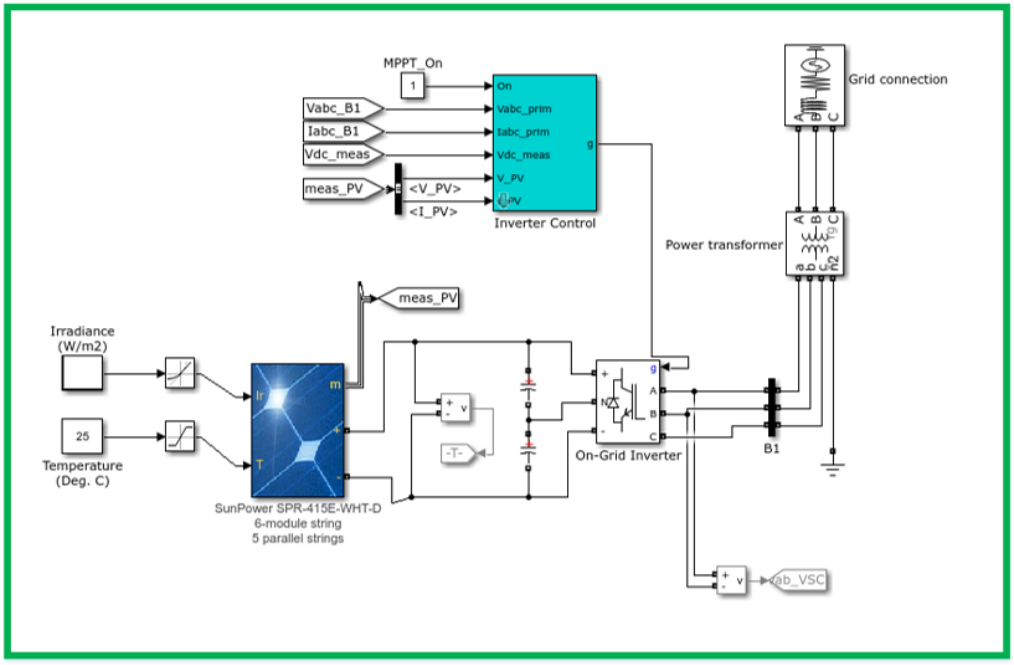

Figure 9. The model of a grid-connected solar PV power plant for a solar-powered smart grid.

The issue that conventional MPPT techniques are trying to solve is how to automatically determine the voltage or current at which a PV array will produce the most electricity at a certain temperature and irradiance. By sampling the solar PV power plant current and voltage, the MPPT algorithm used in the P&O technique determines the solar PV output power and the power change. The calculation of the solar PV power plant output power change over successive cycles is the basis for this approach. The output power value of the solar PV power plant during the current cycle (obtained by measuring both the PV current and voltage values) is contrasted with that of the cycle before. The algorithm determines whether to raise or lower the reference current based on the results of this comparison. If the solar PV power plant output power is rising, the current direction of change will remain unchanged from the prior direction. The direction of change for the current is reversed when the power difference between two consecutive cycles is negative. The output of power oscillates around the peak power at a steady state because the current perturbation is fixed in each cycle.

The main problem of renewable power plants is the occurrence of large imbalances in the produced power and supplied power to the grid under constantly changing weather conditions [58,59]. Overcoming these problems occurring in the grid with the proposed system extends the life of the devices used in smart homes and increases the profits of the smart hosts. In this study, variable solar radiation amounts and variable temperatures are applied to the solar PV panels. Thus, it is aimed to show the changes in power quality affecting the system and the efficiency of the proposed solid-state transformer. Table 2 presents the parameter of the solar PV panel used in the simulation. Figure 10 shows the power changes in solar PV plants under changing weather conditions. With 5 parallel string structures in the solar PV array, the produced voltage can be constant. Since the decrease in the amount of solar radiation causes current losses in the solar cells, the change in power is observed in proportion to the current.

The dc–dc bidirectional DAB converters exhibit superior performance on power conversion due to their low number of components and great controllability. The proposed DAB converter topology is presented in Figure 11. The proposed converter operates in two manners. These are forward and backward power flow. The power flow direction is changed by using phase-shift modulation. The power flow control is achieved by phase-shifted duty square waves. Two inductors are used in the proposed DAB converter. These

are primary leakage inductance (Lp) and magnetizing inductance (Lm). While Lp prevents sudden voltage spikes and reduces current harmonics, Lm reduces the electromagnetic interferences caused by the circulating current in the high-frequency transformer. Thus, the power losses on the power switches and HF transformer are decreased, and the efficiency of the converter is increased. The proposed dc–dc converter parameters are given in Table 3. Two H-bridges are integrated with an HF transformer.

Table 2. The electrical characteristic of the solar PV panel used in the simulation.

Electrical Characteristics	Value	Electrical Characteristics	Value
Power Rating	415 W	Power Density	192.13 W/m^2
Short Circuit Current (I_{sc})	6.21 A	Power Tolerances	0%–+5%
Open Circuit Voltage (V_{oc})	85.6 V	Peak Efficiency	19.66%
Maximum System Voltage	600 V	Nominal Operating Cell Temperature	45.8 °C

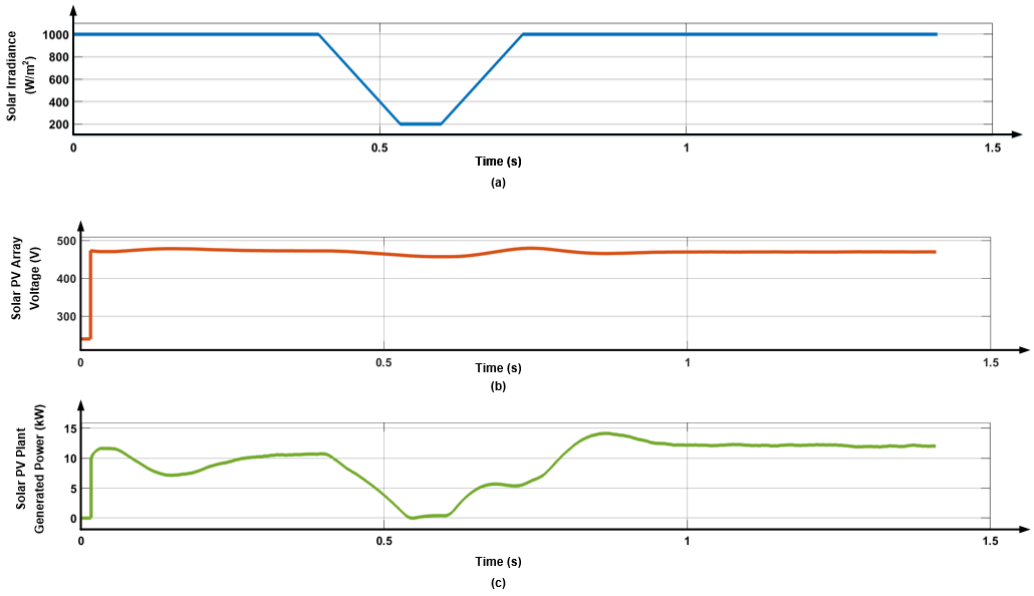

Figure 10. Solar PV power plant: (**a**) solar irradiance, (**b**) PV array voltage, (**c**) generated power.

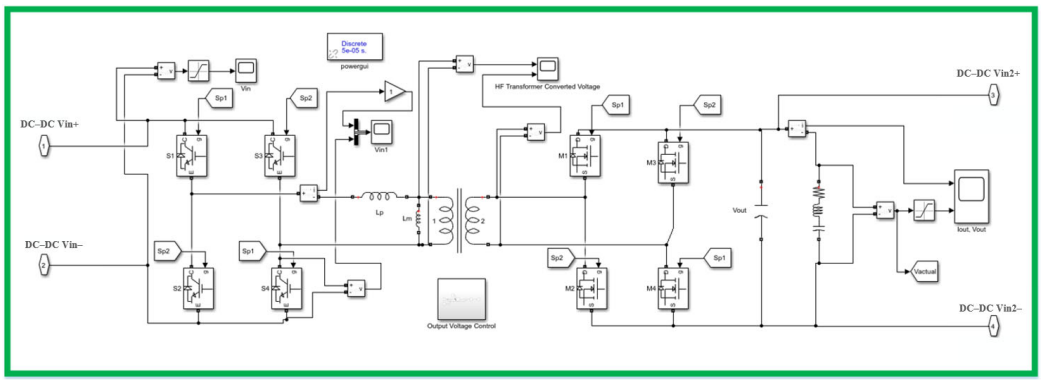

Figure 11. Bidirectional dc–dc DAB converter used for solar PV power plant integrated ST.

To reduce the power switch turn-on and turn-off losses and enable the ZVS operation, 1.2 kV IGBTs are used in the MV side of the converter. 600 V MOSFETS are used in the LV levels under low power level conditions.

Table 3. The proposed DAB converter parameters.

Parameters of DAB Module	**Value**	**Parameters of HF Transformer**	**Value**
Power	12.5 kW	Input Capacitor	0.88 mF
Input Voltage	750 V	Output Capacitor	0.67 mF
Output Voltage & Current	400 V, 30 A	Switching Frequency	20 kHz
Parameters of HF Transformer	**Value**	**Parameters of HF Transformer**	**Value**
Magnetizing Inductance (L_m)	140 mH	Magnetization Resistance (Ω) and Inductance (H)	1.8 kΩ–3 H
Primary Leakage Inductance (L_P)	2.2 mH	Turn ratio (N)	2:1

The controlling operation is the key part of the DAB converter design to gain system stability and higher efficiency of the system. To obtain the desired output voltage from the input voltage, PWM signals are used in the power switches. As shown in Figure 12, the output voltage control is enabled by using the voltage loop control. The output voltage is compared with the reference voltage to obtain the error value. Thus, the difference between the actual dc-link voltage and reference voltage undergoes a PI control and then the limiter to produce the required phase-shift angle and PWM signals. To achieve regulated output voltage, the variable phase angle is applied to the LV-side PWM and MV-side bridges.

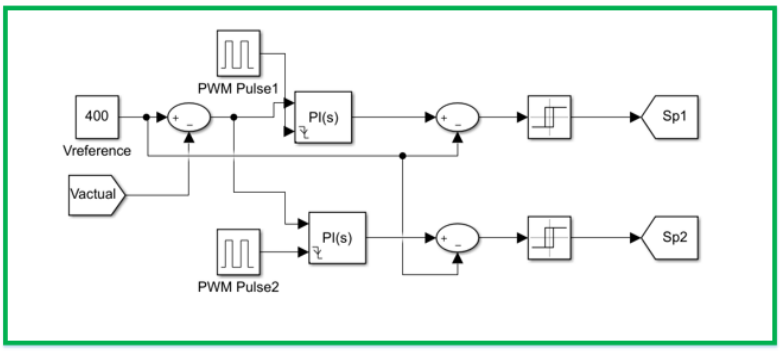

Figure 12. Output voltage control of the proposed DAB converter.

To verify the performance of the voltage control, Figure 13 shows the MV and LV-side capacitor voltages. Although the changing power condition is realized in the solar PV power plant due to the weather condition, voltage stability is provided. Also, an LC filter is applied out of the PWM rectifier to regulate the MV-side capacitor voltage.

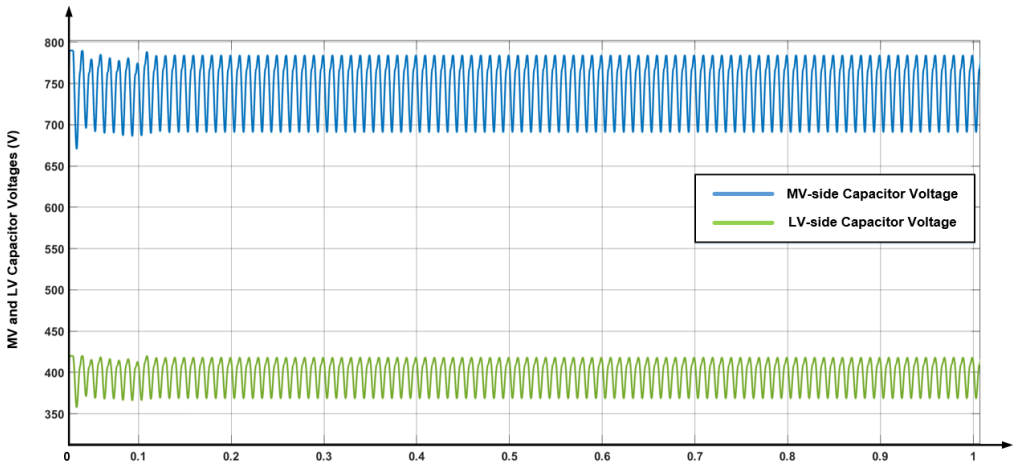

Figure 13. MV and LV side voltages of the DAB converter.

The DAB converter topology is favorable to reduce the switching losses by using ZVS operation. Figure 14 presents the ZVS operation of the proposed converter. The selection of the power switches and control methods plays a key role to achieve the ZVS operation. The waveforms of the MV-side h-bridge output voltage (Vs1) and the output current (Is1) demonstrate the success of the ZVS operation. This isolated converter operates at the resonant point to achieve zero voltage (ZVS) turn-on at the primary side. When the MV-side h-bridge input voltage (VP1) and VS1 reverse polarity, the resonant mode between the transformer leakage inductance and the capacitors (C1 and C2) in parallel with the switches occurs. For example, in Figure 11, switches S2 and S3 are fully turned on and S1 and S4 are at the off state before the period equals zero. At this time, S2 is turned off at zero voltage level (ZVS) while S3 is kept in the on state. Resonance occurs between Lp, C1, and C2. The switch capacitors reset the capacitive energy from S2 to S1. This topology is known as a quasi-resonant ZVS because the resonant operation only occurs for a brief duration of the switching period. The load current is therefore being conducted by diode D1, and switch voltage S2 is Vin1. Now, the resonant inductor is charged by the dc voltage. The active switch is guaranteed to turn on ZVS since the anti-parallel diode is still conducting. S1 is conducting and can be turned off by the control logic to begin the subsequent resonance operation when the load current changes to positive.

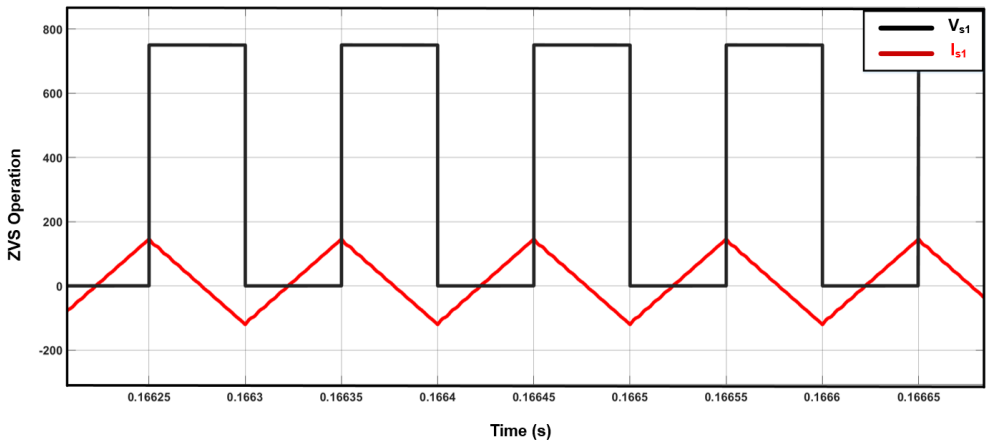

Figure 14. ZVS operation of the bidirectional dc–dc DAB converter.

The essential elements of a DC–AC inverter are depicted in Figure 15. The DC source's ripples or frequency distortions are eliminated by the input filter. It gives the inverter circuit a pure voltage. The primary power circuit of the entire system is the inverter. The desired multilayer PWM waveform is created by this circuit by converting the DC voltage. The output filter helps to create a signal that is almost sinusoidal by attenuating the high-frequency components of the PWM waveform.

In this design, the inverter is controlled by the Sinusoidal Pulse Width Modulation (SPWM) approach because it can directly regulate the output voltage and output frequency in accordance with sine functions. Constant amplitude pulses with variable cycle periods within each period define the SPWM technology. In order to regulate the converter output voltage and lower harmonics, the width of these pulses is varied. Three sine waves and high-frequency triangular carrier waves are used to create the PWM signal in the sinusoidal pulse width modulation approach. The amplitude of the voltage at the converter's output depends on the amplitude modulation rate in the sinusoidal pulse width modulation approach. Overmodulation and distorted sinusoidal PWM output results from raising the modulation ratio at the high output voltage closer to 1. The output voltage must have its frequency and amplitude adjusted by the inverter. Pulse width modulation provides this adjusting mechanism. An inverter's output voltage must have its amplitude and frequency modified. The output voltage should be as near to the sinus form as possible while these are

set. The frequency of the control signal must match the intended frequency at the output in order to produce a sinusoidal voltage at that frequency.

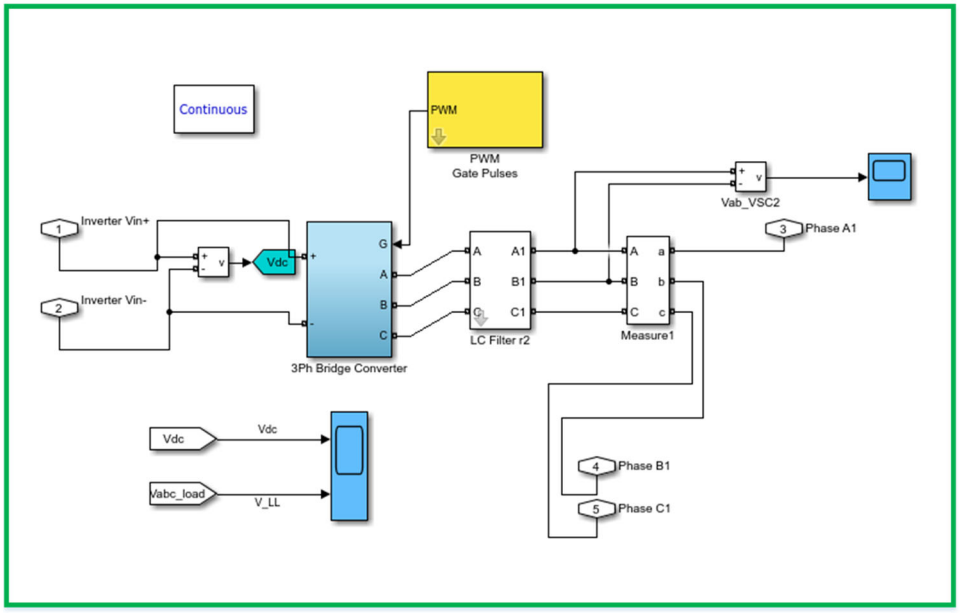

Figure 15. PWM inverter for DC–AC stage of the ST.

The end-user obtains pure electricity for the home. The most important part of the efficient use of electricity is realized by the proposed dc–dc converter structure. Increasing the power quality and ensuring power control provides efficient electricity output. In ideal conditions, it is hard to obtain the pure electrical waveforms in a renewable energy-connected electric grid, but this case can be possible thanks to the proposed DAB converter-based ST in a renewable energy integrated grid system as shown in Figure 16.

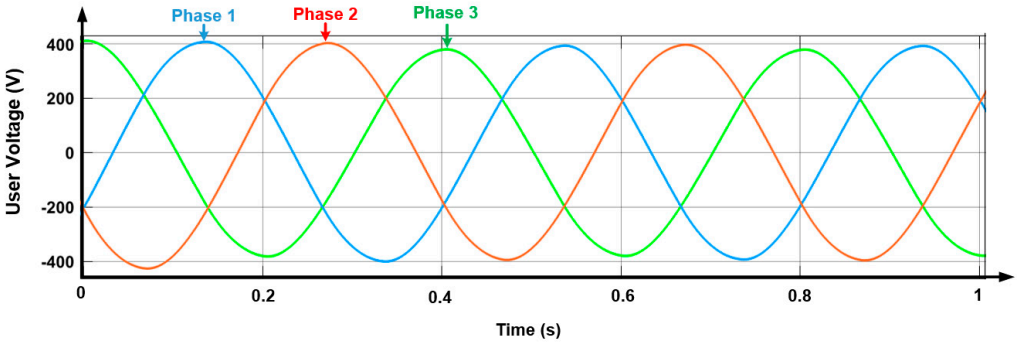

Figure 16. End-user regulated voltage.

3.2. Experimental Model

The gate driver circuit is an integral part of power electronics systems. Gate drivers form an important interface between high-power electronics and control circuitry and are used to drive power semiconductor devices. The output of DA–DA converters or SMPS mainly depends on the behavior of the gate driver circuits. Therefore, the design of the gate driver circuit is critical in the design of power electronics converters. In this study, an HCPL 3120 gate driver is used to drive the high-power IGBT. A GaAsP LED is included inside the HCPL-3120 gate driver optocouplers. A power output stage-equipped integrated circuit is optically connected to the LED, ideal for providing driving power to MOSFETs and IGBTs for inverted motor control applications. The output stage's high operating voltage range supplies the drive voltages needed by gate-controlled devices.

It is the best option for driving IGBTs rated up to 1200 V/100 A due to the voltage and current offered. The HCPL-3120 series can be utilized to drive a separate power stage driving the IGBT gate for higher-rated IGBTs. It features a 630 V peak insulation voltage. Figure S5 depicts the HCPL-3120's application circuit for driving the IGBT.

To drive high-power Mosfets, a driver circuit was created with the IR2104 IC together with a 4N25 isolated optocoupler. The typical connection structure of the Mosfet driver circuit is presented in Figure S6.

DAB bidirectional DC/DC converter is a topology with the advantages of reduced device count, soft-switched commutations, low cost, and high efficiency. The use of this topology is recommended for applications where power density, cost, weight, and reliability are critical factors. The Phase Shift Modulation method, which is frequently preferred in the literature, has been applied to generate trigger signals in the DA–DA Converter control algorithm. The advantage of Phase Shift Modulation is that it allows high power transfer capacity between converters and is suitable for use for variable DC link voltages. If the DC link voltages are constant and close to each other in accordance with the transformer conversion ratio, it provides maximum efficiency. The proposed dual-direction DAB converter was designed and produced as an H bridge. The designed DAB converter card design and the produced card are shown in Figure 17.

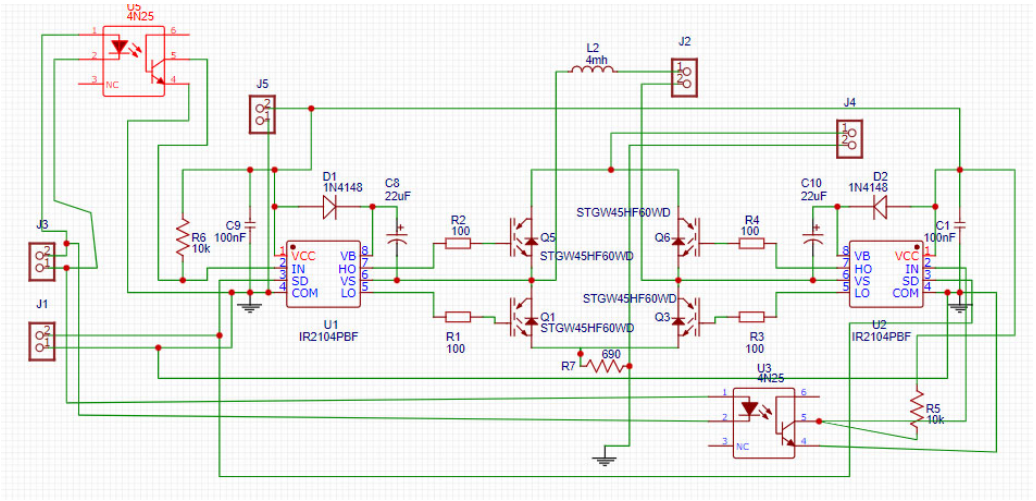

(**a**)

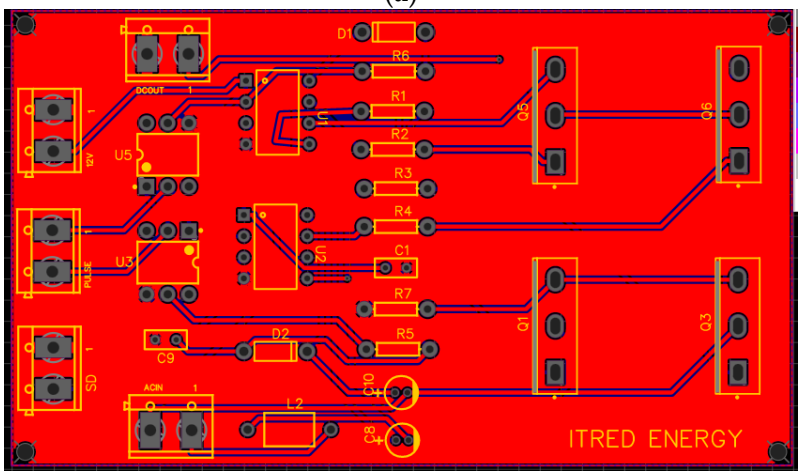

(**b**)

Figure 17. Designed primary and secondary circuits of DAB converter: (**a**) circuit diagram, (**b**) 2D card view.

To drive the IGBT key elements at high speed, the driving process is carried out with the additional design of the HCPL-3120 IC for the PWM inverter. When IGBTs operate at high current and voltage values, an isolated driver model is used to prevent the control card from burning against reverse current flow. Gate signals with a 50% duty cycle are used for each IGBT. The control card driver test circuit is carried out on the PCB on the experimental table. It is designed with a PCB card by designing an isolated gate driver. In Figure 18, the designed gate driver model for one module is given.

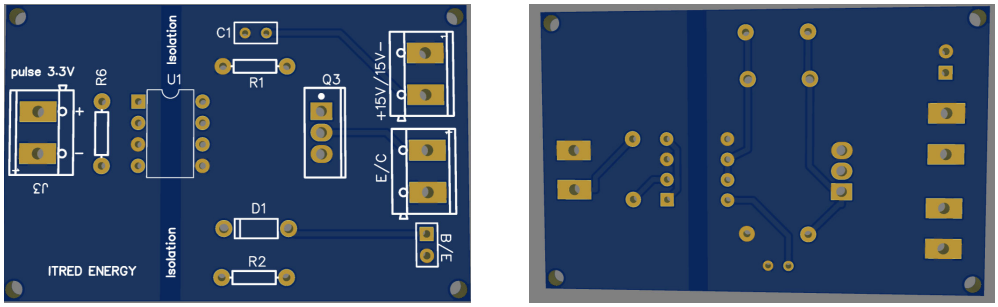

(**a**) (**b**)

Figure 18. Isolated gate driver circuit for one IGBT module: (**a**) front view, (**b**) rear view.

The gate signals required to drive the IGBTs after the isolated driver circuit is as in Figure 19. With the circuit proposed in Figure 19, the signals operate at a switching speed below 600 ns.

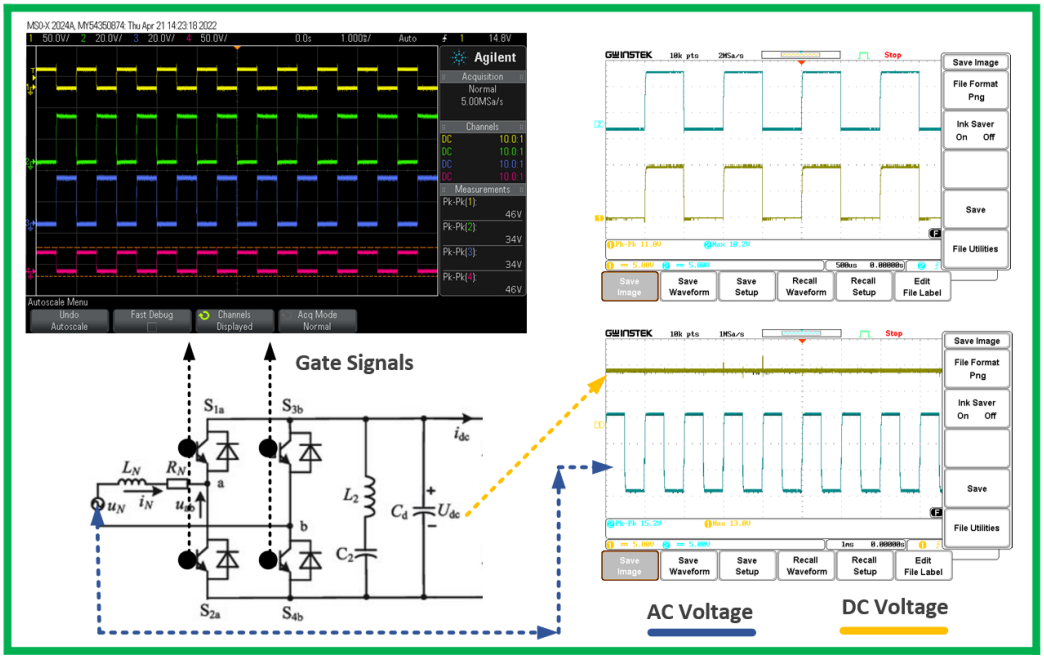

Figure 19. Isolated gate PWM inverter structure gate signals, and dc input and ac output signals.

Mosfet and IGBT drivers need dc feeds in converter, converter, and inverter card designs. Card designs are produced piece by piece in isolation so that they are not affected by electromagnetic interference. With a single 5 V dc supply, different voltage dc supplies of the drivers are provided in isolation on all cards. Being isolated is important for the earthing problem, harmonic fluctuations, and short circuit protections in the cards. These problems are eliminated with the multi-output isolated DC supply design. With the voltage that we get 5 V supply from the control card, the feeds are given to the converter cards with a single voltage without the need for external dc voltages. The 5 V voltage coming

from the control card is first passed through insulated dc–dc (5 V–5 V) converters to ensure ground isolation. In Figure S7, an isolated dc–dc design circuit is presented.

The isolated DC/DC converter is typically used in cost-sensitive general-purpose power isolation and voltage-matching applications. Despite its low cost, a full-featured converter with 1 kVDC isolation and an industrial operating temperature range of −40 °C to +85 °C is used.

Adjustable supply voltage between 5 V–50 V is provided by XL6009 IC. The XL6009 regulator is a wide input range, current mode, and DC/DC converter that can generate positive or negative output voltages. It can be configured as Boost, flyback, SEPIC, or inverting converter. The XL6009 built-in N-channel power MOSFET, fixed frequency oscillator, and current mode architecture ensure stable operation over a wide range of supply and output voltages. The application circuit is given in Figure S8. The isolated dc card feeds design is given in Figure S9.

The 10 kVA 380–380 V soft switching smart transformer model is presented in Figure 20. The model consists of a rectifier circuit, DAB converter, and PWM inverter. Variable AC voltage produced by a solar PV power plant is converted and controlled by the smart transformer to enable user voltage.

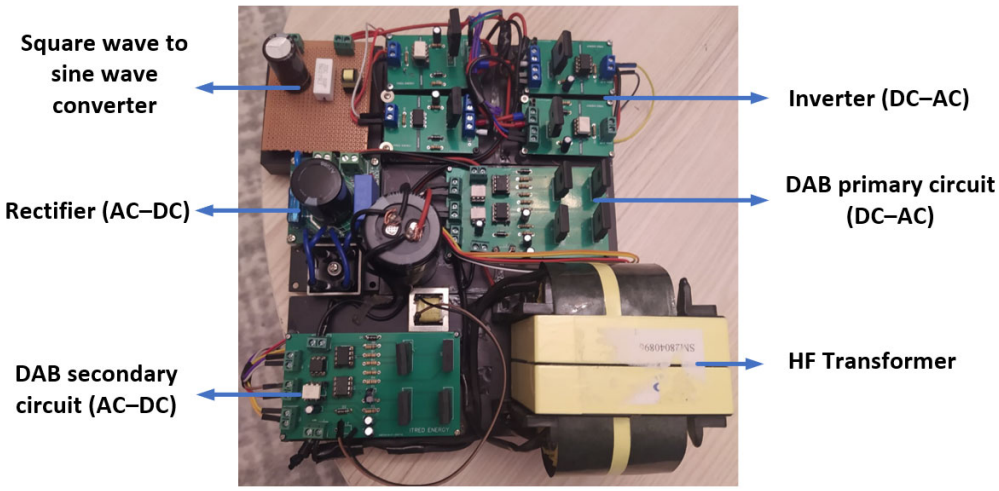

Figure 20. Designed and produced smart transformer model for smart power grids.

Power measurements, signal conditioning unit with amplifiers, and supply voltage for converters and inverters are given in Figure 21. The main voltage is obtained from the output power of the solar PV power plant. This voltage is reduced to 12 Vac by a 10 W, 220/12 Vac power transformer. The 12 Vac voltage is converted to 5 Vdc with the diode rectifier circuit. The 5 Vdc voltage is also converted to multi-output supply voltages with isolated dc–dc converters. The 5 Vdc supply voltages are increased up to 50 Vdc with the help of a boost converter, providing supply voltages for converters and inverters. In the measurement and signal conditioning circuit, the reference voltage (220 Vac) is converted to 5 Vac with the current/voltage measurement sensor. The 5 Vac obtained from the sensor is converted to the 3.3 Vac unipolar signal allowed by the DSP control card with the signal scaling circuit. The current/voltage and PWM control in the DSP control card is provided by control blocks via MATLAB/Simulink.

With 220 Vac supply voltage, the ST converted the ac–dc converter side to 450 Vdc voltage. Based on the 450 Vdc voltage, the final conversion voltage in the inverter part is 220 V according to the transformer conversion ratio. When the conversion efficiencies of the DAB converter and ST are calculated, they are recorded as 98.6% and 96.7% at 10 kVA. The input voltage obtained with the solar PV power plant passes through the smart transformer. Here, controlled power is sent to the end-user smart grid by controlling the variable input voltage. Figure 22 presents that the waveforms of the input and output voltages are given sequentially.

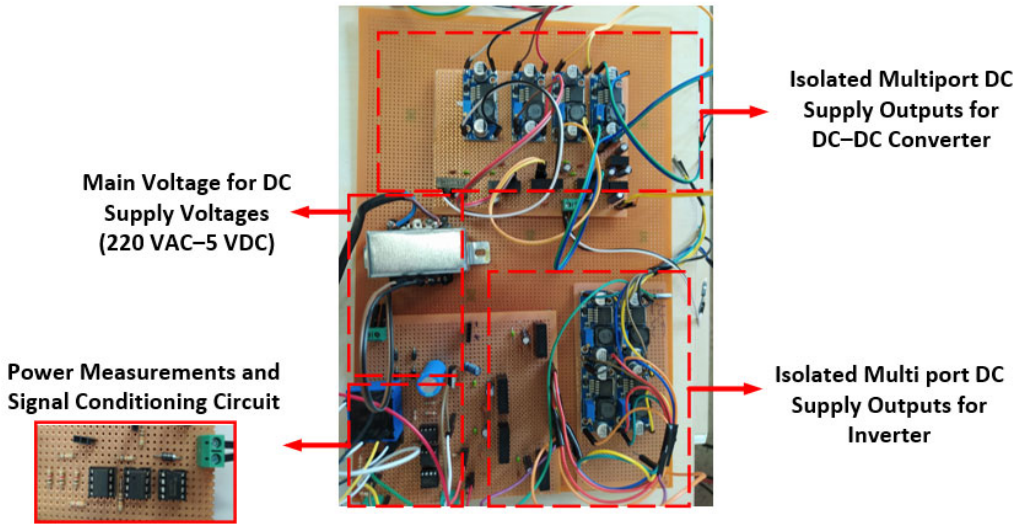

Figure 21. Power measurement, supply voltage circuit, and signal conditioning circuit for smart transformer.

Soft switching means eliminating the on or off switching losses of one or more power switches in a dc-to-dc converter. Soft switching capability means that the proposed circuit has full range ZVS, which is better than conventional solutions with no ZVS or only limited range ZVS in DAB. Figure 23 shows the experimental results for the ZVS (zero switching) gain taken across the high voltage side of the HFT, corresponding to a current of 10.4 A on the primary side.

The high-frequency oscillation issue brought on by the transformer's capacitances and the dual active bridge (DAB) converter's high dv/dt increases in severity with higher switching speed. Theoretically, the zero crossing points of the DAB dv/dt excitation might be positioned at the oscillation frequency to solve the high-frequency oscillation problem. By connecting parallel capacitors to the power components, the DAB dv/dt is changed. The transformer's reduced oscillation loss and superior soft-switching conditions not only solve the high-frequency oscillation issue, but also allow for an increase in efficiency. Short rise times can cause high dv/dt, which can cause voltage spikes and ringing on the voltage pulse's leading edge. This ringing is a high-frequency EMI source, and if the peak voltage is sufficiently high, the voltage spikes could harm the loads. The resonant capacitor controls the dv/dt in the proposed converter, whereas the DAB only controls the dv/dt within its ZVS range and the dv/dt of the inverter is uncontrolled. Devices made of MV SiC can have uncontrolled dv/dt rates of up to 10–100 kV/s [60]. The dv/dt rate of 6.8 kV/us is validated by experimental data using a 344 Vac 10.4 A load current. The dv/dt analysis is shown in Figure 24.

The ST performance in the sudden sag and swell of the power produced from the 12.5 kW solar PV power plant is presented in Figure 25 with current voltage measurements of the ST output. Considering the signal fluctuations, it is observed that the end-user output voltage is kept constant, and no visible harmonics occur in the load current.

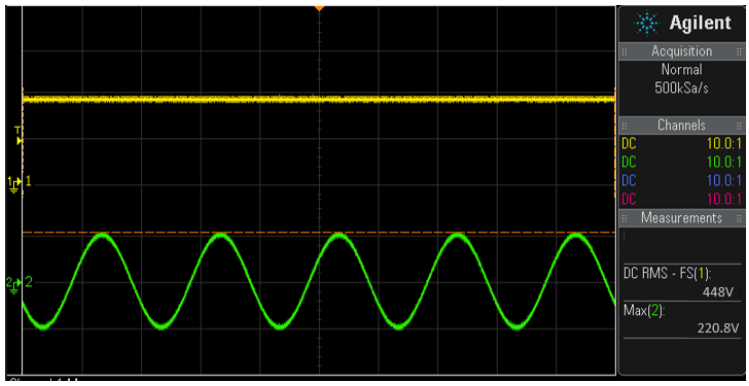

(**a**)

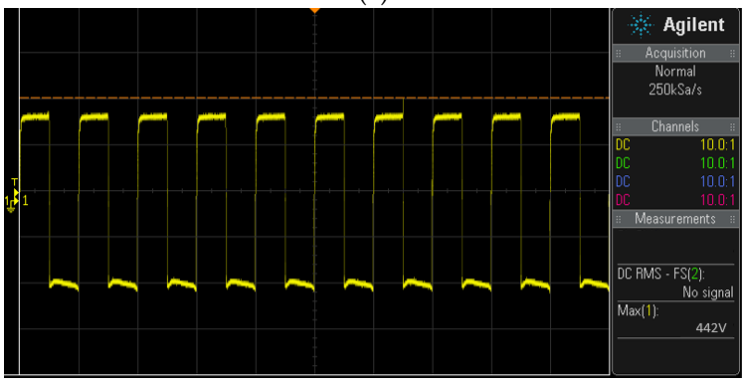

(**b**)

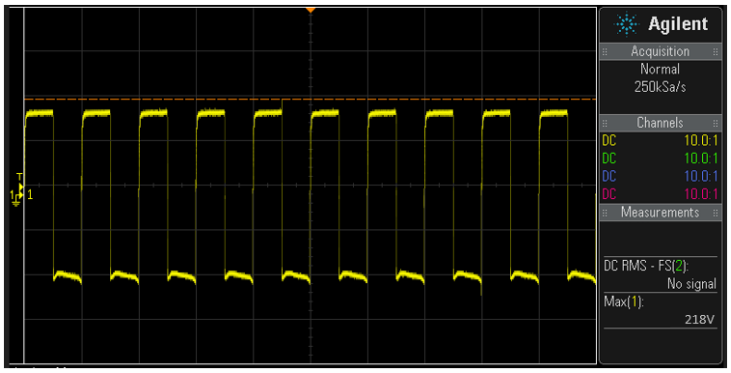

(**c**)

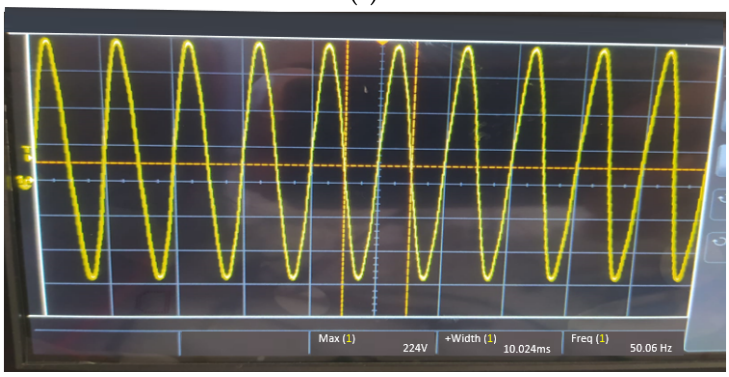

(**d**)

Figure 22. Sequence display of system power outputs: (**a**) AC–DC rectifier input voltage and converted dc voltage, (**b**) the voltage converted to alternating current in the primary part of the HF transformer, (**c**) AC voltage at the secondary of the HF transformer, (**d**) inverter output voltage.

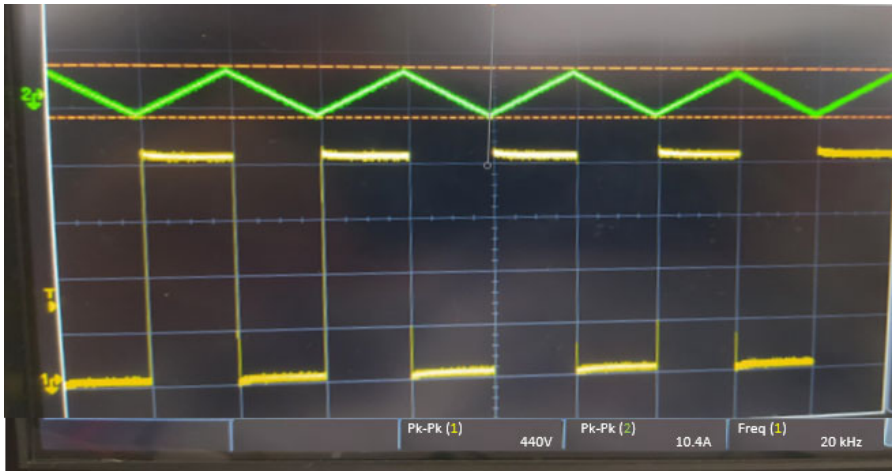

(**a**)

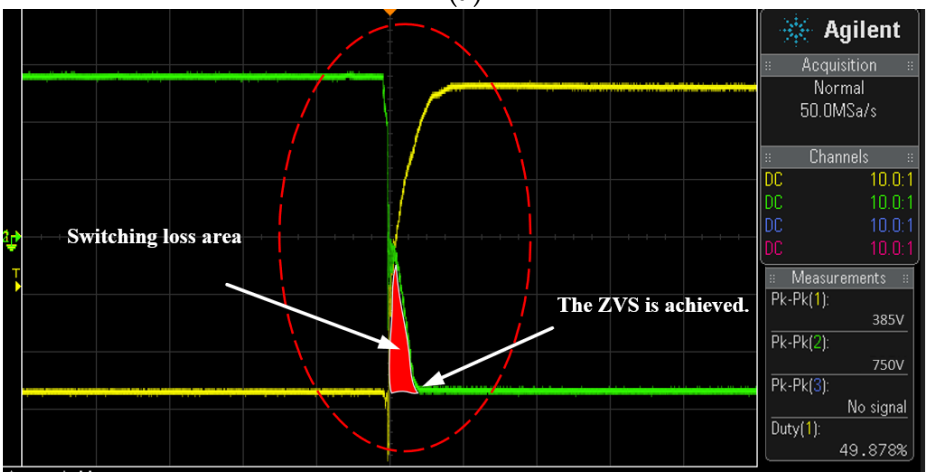

(**b**)

Figure 23. ZVS gain: (**a**) HF transformer primary side, (**b**) Switch voltage measurements to verify the ZVS.

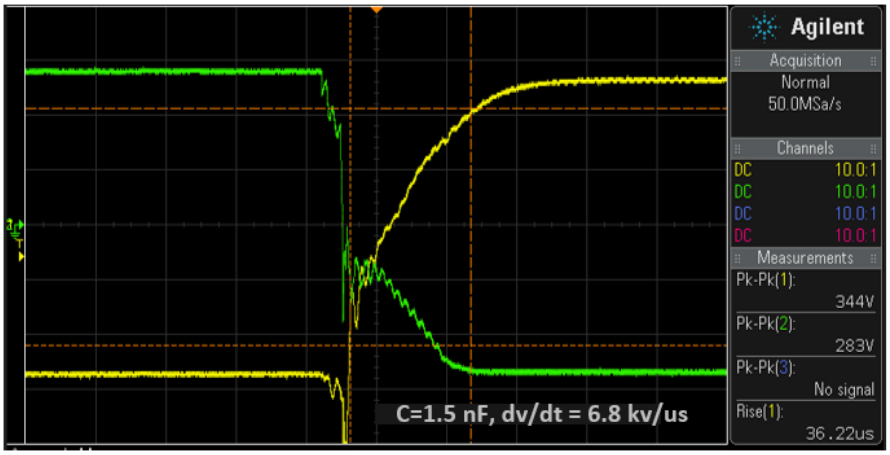

Figure 24. The controlled dv/dt across the reverse-blocking switches.

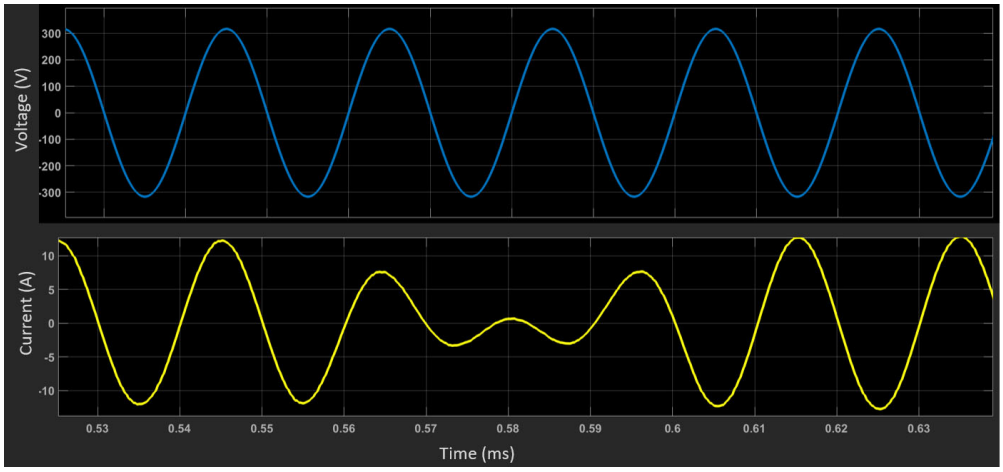

Figure 25. Output power of the ST under the sudden sag and swell of the Solar PV power.

4. Conclusions

The demand for renewable energy is increasing day by day, thus the increase of renewable energy integration needs improvements on the controllability side. STs are potential solutions to enable power flow control, reactive power compensation, harmonic control, ac–dc–dc–ac conversion, and renewable integration. The isolation stage is the main part of the ST due to the gain of higher efficiency and controllability to the system. With a comprehensive literature survey, the dc–dc converter topologies used in different ST applications are examined. However, the optimal dc–dc converter topology selection for grid-connected solar PV power plants has not been discussed in the literature.

Under the rated load condition, the proposed DAB converter runs at the fixed resonant frequency with a 50% duty cycle. To reduce the backflow power and switch on-off current, the magnetizing inductance (Lm) can be increased. Yet, magnetizing inductance should be small enough to achieve the ZVS operation. Also, extending the deadband period results in a larger magnetizing inductance to meet the optimal ZVS requirement. This case can reduce the backflow power, but it leads to a reduction in the effective time for energy transfer. The balance between the magnetizing inductance and the dead time specifies the ZVS operation performance of the DAB. The switching power losses are reduced by extending the ZVS range and adopting a control strategy. The selection of the power switches and HF transformer parameters is significant to reduce the circulating current. The 10 kVA 380/380 Vac ST experimentally tested in terms of reduced dv/dt, ZVS gain, and conversion efficiency at variable voltages. The dv/dt rate of 6.8 kV/us is achieved by experimental data using a 344 Vac 10.4 A load current. ZVS gain is observed at HF transformer primary side and switch voltage measurements to verify the success. The conversion efficiency is calculated at 96.7% at full load conditions. The switching loss is close to ideal when looking at the ZVS gain in dynamic analysis. In the experimental analysis, switch losses at full load are clearly visible. In the experimental study, the ST output power was observed as 9.66 kW at 750 Vac peak to peak voltage and 12.89 A current, and in dynamic analysis it was 9.9 kW at 750 Vac voltage and 13.2 A current. In the experimental study and dynamic analysis, the ST efficiency was 96.67% and 99%, respectively. In this experimental study, it is seen that besides the switching losses, there are also transmission losses and HF transformer losses. The proposed ST has potentially reduced EMI from controlled dv/dt and full-range ZVS capability Also, the control system gives better performance on the dc voltage stability and presents a safe operation. The proposed ST has potentially reduced EMI from controlled dv/dt and full-range ZVS capability. With a useful control method, voltage balancing between the converter modules under the steady-state and the dynamic conditions is achieved.

Supplementary Materials: The following supporting information can be downloaded at: https://www.mdpi.com/article/10.3390/su15010032/s1.

Author Contributions: Conceptualization, B.E. and T.D.; methodology, B.E.; software, B.E.; validation, B.E. and T.D.; formal analysis, B.E. and T.D.; investigation, B.E. and T.D.; resources, T.D.; data curation, B.E.; writing—original draft preparation, B.E. and T.D.; writing—review and editing, B.E. and T.D.; visualization, B.E.; supervision, T.D.; project administration, T.D.; funding acquisition, T.D. All authors have read and agreed to the published version of the manuscript.

Funding: This research was supported by the Scientific Project Unit of Adana Alparslan Türkeş Science and Technology University (Project Number: 20803001) and the Scientific and Technological Research Council of Turkey (TÜBİTAK Project Number: 2210319).

Institutional Review Board Statement: Not applicable.

Informed Consent Statement: Not applicable.

Data Availability Statement: Not applicable.

Conflicts of Interest: The authors declare no conflict of interest.

Abbreviations

EMI	Electromagnetic interference	SRC	Series resonant converter
ST	Smart transformer	MV	Medium voltage
OLC	open-loop control	LV	Low voltage
ISOP	Input series output parallel	QAB	Quadruple-Active-Bridge
ZVS	Zero voltage switching	PWM	Pulse width modulation
ZCS	Zero current switching	RMS	Root mean square
DAB	Dual Active Bridge	PV	Photovoltaic
PR	Proportional resonant controller	ADC	Analog to Digital
Q2L	Quasi-2-Level	MPPT	Maximum power point
HF	High frequency	SPWM	Sinusoidal pulse width modulation
HFT	High frequency transformer	P&O	Perturb and observe

References

1. Li, Y.; Han, J.; Cao, Y.; Li, Y.; Xiong, J.; Sidorov, D.; Panasetsky, D. A Modular Multilevel Converter Type Solid State Transformer with Internal Model Control Method. *Int. J. Electr. Power Energy Syst.* **2017**, *85*, 153–163. [CrossRef]
2. Zhang, J.; Wang, Z.; Shao, S. A Three-Phase Modular Multilevel DC–DC Converter for Power Electronic Transformer Applications. *IEEE J. Emerg. Sel. Topics Power Electron.* **2017**, *5*, 140–150. [CrossRef]
3. Li, Y.; Lyu, X.; Cao, D. A Zero-Current-Switching High Conversion Ratio Modular Multilevel DC–DC Converter. *IEEE J. Emerg. Sel. Topics Power Electron.* **2017**, *5*, 151–161. [CrossRef]
4. Kadandani, N.B.; Dahidah, M.; Ethni, S. Design and Development of Modular Multilevel Converter for Solid State Transformer Application. *Bayero J. Eng. Technol.* **2021**, *16*, 31–41.
5. Alam, K.S.; Tria, L.A.R.; Zhang, D.; Xiao, D.; Rahman, M.F. Multi-Cell DC-DC Converter Based Solid-State Transformer (SST) Design Featuring Medium-Voltage Grid-Tie Application. In Proceedings of the 2017 20th International Conference on Electrical Machines and Systems (ICEMS), Sydney, Australia, 11–14 August 2017; IEEE: Piscataway, NJ, USA, 2017; pp. 1–6.
6. Chen, Y.; Li, Y.; Zhu, M. A Developed Dual MMC Isolated DC Solid State Transformer and Its Modulation Strategy. In Proceedings of the International Power Electronics Conference (ECCE Asia), Niigata, Japan, 20–24 May 2018.
7. Jiao, Y.; Jovanović, M.M. Topology Evaluation and Comparison for Isolated Multilevel DC/DC Converter for Power Cell in Solid State Transformer. In Proceedings of the 2019 IEEE Applied Power Electronics Conference and Exposition (APEC), Anaheim, CA, USA, 17–21 March 2019; pp. 802–809.
8. Liu, C.; Li, X.; Zhi, Y.; Cai, G. New Breed of Solid-State Transformer Mainly Combing Hybrid Cascaded Multilevel Converter with Resonant DC-DC Converters. *Appl. Energy* **2018**, *210*, 724–736. [CrossRef]
9. Wang, L.; Zhu, Q.; Yu, W.; Huang, A.Q. A Medium Voltage Bidirectional DC-DC Converter Combining Resonant and Dual Active Bridge Converters. In Proceedings of the 2015 IEEE Applied Power Electronics Conference and Exposition (APEC), Charlotte, NC, USA, 15–19 March 2015; IEEE: Piscataway, NJ, USA, 2015; pp. 1104–1111.
10. Huber, J.E.; Kolar, J.W. Analysis and Design of Fixed Voltage Transfer Ratio DC/DC Converter Cells for Phase-Modular Solid-State Transformers. In Proceedings of the 2015 IEEE Energy Conversion Congress and Exposition (ECCE), Montreal, QC, Canada, 20–24 September 2015; IEEE: Piscataway, NJ, USA, 2015; pp. 5021–5029.

11. Ortiz, G.; Leibl, M.G.; Huber, J.E.; Kolar, J.W. Design and Experimental Testing of a Resonant DC–DC Converter for Solid-State Transformers. *IEEE Trans. Power Electron.* **2017**, *32*, 7534–7542. [CrossRef]
12. Costa, L.; Buticchi, G.; Liserre, M. Bidirectional Series-Resonant DC-DC Converter with Fault-Tolerance Capability for Smart Transformer. In Proceedings of the 2016 IEEE Energy Conversion Congress and Exposition (ECCE), Milwaukee, WI, USA, 18–22 September 2016; IEEE: Piscataway, NJ, USA, 2016; pp. 1–7.
13. Costa, L.F.; Buticchi, G.; Liserre, M. Highly Efficient and Reliable SiC-Based DC–DC Converter for Smart Transformer. *IEEE Trans. Ind. Electron.* **2017**, *64*, 8383–8392. [CrossRef]
14. Zhao, S.; Li, Q.; Lee, F.C.; Li, B. High-Frequency Transformer Design for Modular Power Conversion from Medium-Voltage AC to 400 VDC. *IEEE Trans. Power Electron.* **2018**, *33*, 7545–7557. [CrossRef]
15. Lai, J.-S.; Choe, J.M.; Yeh, C.-S.; Moon, S.-R.; Lai, W.-H.; Zhang, L. A Modular Front-End Medium-Voltage Solid-State Transformer. In Proceedings of the 2017 Asian Conference on Energy, Power and Transportation Electrification (ACEPT), Singapore, 24–26 October 2017; IEEE: Piscataway, NJ, USA, 2017; pp. 1–6.
16. Yeh, C.-S.; Zhang, L.; Choe, J.-M.; Chen, C.-W.; Yu, O.; Lai, J.-S. Light-Load Efficiency Improvement for LLC Converter with Synchronous Rectification in Solid-State Transformer Application. In Proceedings of the 2018 IEEE Applied Power Electronics Conference and Exposition (APEC), San Antonio, TX, USA, 4–8 March 2018; IEEE: Piscataway, NJ, USA, 2018; pp. 2142–2147.
17. Dong, D.; Agamy, M.; Bebic, J.Z.; Chen, Q.; Mandrusiak, G. A Modular SiC High-Frequency Solid-State Transformer for Medium-Voltage Applications: Design, Implementation, and Testing. *IEEE J. Emerg. Sel. Top. Power Electron.* **2019**, *7*, 768–778. [CrossRef]
18. Lu, Z.; Li, C.; Zhu, A.; Luo, H.; Li, C.; Li, W.; He, X. Medium Voltage Soft-Switching Dc/Dc Converter with Series-Connected Sic MOSFETs. *IEEE Trans. Power Electron.* **2020**, *36*, 1451–1462. [CrossRef]
19. Tripathi, A.K.; Mainali, K.; Patel, D.C.; Kadavelugu, A.; Hazra, S.; Bhattacharya, S.; Hatua, K. Design Considerations of a 15-KV SiC IGBT-Based Medium-Voltage High-Frequency Isolated DC–DC Converter. *IEEE Trans. Ind. Appl.* **2015**, *51*, 3284–3294. [CrossRef]
20. Madhusoodhanan, S.; Tripathi, A.; Patel, D.; Mainali, K.; Kadavelugu, A.; Hazra, S.; Bhattacharya, S.; Hatua, K. Solid-State Transformer and MV Grid Tie Applications Enabled by 15 KV SiC IGBTs and 10 KV SiC MOSFETs Based Multilevel Converters. *IEEE Trans. Ind. Appl.* **2015**, *51*, 3343–3360. [CrossRef]
21. Rothmund, D.; Ortiz, G.; Guillod, T.; Kolar, J.W. 10 kV SiC-Based Isolated DC-DC Converter for Medium Voltage-Connected Solid-State Transformers. In Proceedings of the 2015 IEEE Applied Power Electronics Conference and Exposition (APEC), Charlotte, NC, USA, 15–19 March 2015; IEEE: Piscataway, NJ, USA, 2015; pp. 1096–1103.
22. Wang, L.; Zhang, D.; Wang, Y.; Wu, B.; Athab, H.S. Power and Voltage Balance Control of a Novel Three-Phase Solid-State Transformer Using Multilevel Cascaded H-Bridge Inverters for Microgrid Applications. *IEEE Trans. Power Electron.* **2016**, *31*, 3289–3301. [CrossRef]
23. Choi, H.-J.; Park, H.-P.; Jung, J.-H. Design Methodology of Dual Active Bridge Converter for Solid State Transformer Application in Smart Grid. In Proceedings of the 2015 9th International Conference on Power Electronics and ECCE Asia (ICPE-ECCE Asia), Seoul, Republic of Korea, 1–5 June 2015; IEEE: Piscataway, NJ, USA, 2015; pp. 196–201.
24. Lopez, M.; Rodriguez, A.; Blanco, E.; Saeed, M.; Martinez, A.; Briz, F. Design and Implementation of the Control of an MMC-Based Solid State Transformer. In Proceedings of the 2015 IEEE 13th International Conference on Industrial Informatics (INDIN), Cambridge, UK, 22–24 July 2015; IEEE: Piscataway, NJ, USA, 2015; pp. 1583–1590.
25. Bahmani, M.A.; Thiringer, T.; Kharezy, M. Optimization and Experimental Validation of Medium-Frequency High Power Transformers in Solid-State Transformer Applications. In Proceedings of the 2016 IEEE Applied Power Electronics Conference and Exposition (APEC), Long Beach, CA, USA, 20–24 March 2016; IEEE: Piscataway, NJ, USA, 2016; pp. 3043–3050.
26. Wang, Q.; Liang, D. Research on Loss Reduction of Dual Active Bridge Converter over Wide Load Range for Solid State Transformer Application. In Proceedings of the 2016 Eleventh International Conference on Ecological Vehicles and Renewable Energies (EVER), Monte Carlo, Monaco, 6–8 April 2016; IEEE: Piscataway, NJ, USA, 2016; pp. 1–9.
27. Ye, Q.; Mo, R.; Li, H. Impedance Modeling and Verification of a Dual Active Bridge (DAB) DC/DC Converter Enabled DC Microgrid in FREEDM System. In Proceedings of the 2016 IEEE 8th International Power Electronics and Motion Control Conference (IPEMC-ECCE Asia), Hefei, China, 22–26 May 2016; IEEE: Piscataway, NJ, USA, 2016; pp. 2875–2879.
28. Zhao, B.; Song, Q.; Li, J.; Liu, W. A Modular Multilevel DC-Link Front-to-Front DC Solid-State Transformer Based on High-Frequency Dual Active Phase Shift for HVDC Grid Integration. *IEEE Trans. Ind. Electron.* **2017**, *64*, 8919–8927. [CrossRef]
29. Liu, J.; Yang, J.; Zhang, J.; Nan, Z.; Zheng, Q. Voltage Balance Control Based on Dual Active Bridge DC/DC Converters in a Power Electronic Traction Transformer. *IEEE Trans. Power Electron.* **2018**, *33*, 1696–1714. [CrossRef]
30. Wen, H.; Chen, J. Control and Efficiency Optimization of Dual-Active-Bridge DC/DC Converter. In Proceedings of the 2016 IEEE International Conference on Power Electronics, Drives and Energy Systems (PEDES), Trivandrum, India, 14–17 December 2016; IEEE: Piscataway, NJ, USA, 2016; pp. 1–6.
31. Wang, L.; Zhang, D.; Wang, Y.; Liu, H. High-Frequency Solid-State Transformer Power Conversion Technologies for Energy Internet. In Proceedings of the 2017 IEEE 3rd International Future Energy Electronics Conference and ECCE Asia (IFEEC 2017—ECCE Asia), Kaohsiung, Taiwan, 3–7 June 2017; IEEE: Piscataway, NJ, USA, 2017; pp. 1397–1401.

32. Zhang, F.; Ma, X.; Huang, L.; Xu, P.; Xuan, Y.; Yang, X.; Hao, X.; Li, Z. Design and Demonstration of a SiC-Based 800-V/10-KV 1-MW Solid-State Transformer for Grid-Connected Photovoltaic Systems. In Proceedings of the 2017 IEEE 3rd International Future Energy Electronics Conference and ECCE Asia (IFEEC 2017—ECCE Asia), Kaohsiung, Taiwan, 3–7 June 2017; IEEE: Piscataway, NJ, USA, 2017; pp. 1987–1990.
33. Mainali, K.; Tripathi, A.; Madhusoodhanan, S.; Kadavelugu, A.; Patel, D.; Hazra, S.; Hatua, K.; Bhattacharya, S. A Transformerless Intelligent Power Substation: A Three-Phase SST Enabled by a 15-KV SiC IGBT. *IEEE Power Electron. Mag.* **2015**, *2*, 31–43. [CrossRef]
34. Briz, F.; Lopez, M.; Rodriguez, A.; Zapico, A.; Arias, M.; Diaz-Reigosa, D. MMC Based SST. In Proceedings of the 2015 IEEE 13th International Conference on Industrial Informatics (INDIN), Cambridge, UK, 22–24 July 2015; IEEE: Piscataway, NJ, USA, 2015; pp. 1591–1598.
35. Shuyu, C.; Sriram, V.B.; Dehghani Tafti, H.; Ravi Kishore, K.V.; Li, Y.H.; Tripathi, A.; Pou, J. Modular DAB DC-DC Converter Low Voltage Side Dc Link Capacitor Two-Stage Charging-up Control for Solid State Transformer Application. In Proceedings of the 2017 Asian Conference on Energy, Power and Transportation Electrification (ACEPT), Singapore, 24–26 October 2017; IEEE: Piscataway, NJ, USA, 2017; pp. 1–7.
36. Gajowik, T.; Sobol, C.; Styński, S.; Malinowski, M. Post-Fault Operation of Hybrid DC-DC Converter for Solid-State Transformer. In Proceedings of the IECON 2017—43rd Annual Conference of the IEEE Industrial Electronics Society, Beijing, China, 29 October–1 November 2017; IEEE: Piscataway, NJ, USA, 2017; pp. 5373–5379.
37. Shi, H.; Wen, H.; Chen, J.; Hu, Y.; Jiang, L.; Chen, G.; Ma, J. Minimum-Backflow-Power Scheme of DAB-Based Solid-State Transformer with Extended-Phase-Shift Control. *IEEE Trans. Ind. Appl.* **2018**, *54*, 3483–3496. [CrossRef]
38. Raveendran, V.; Andresen, M.; Liserre, M.; Buticchi, G. Lifetime-Based Power Routing of Smart Transformer with CHB and DAB Converters. In Proceedings of the 2018 IEEE Applied Power Electronics Conference and Exposition (APEC), San Antonio, TX, USA, 4–8 March 2018; IEEE: Piscataway, NJ, USA, 2018; pp. 3523–3529.
39. Pugliese, S.; Andresen, M.; Mastromauro, R.A.; Buticchi, G.; Stasi, S.; Liserre, M. A New Voltage Balancing Technique for a Three-Stage Modular Smart Transformer Interfacing a DC Multibus. *IEEE Trans. Power Electron.* **2019**, *34*, 2829–2840. [CrossRef]
40. Anurag, A.; Acharya, S.; Prabowo, Y.; Jakka, V.; Bhattacharya, S. Design of a Medium Voltage Mobile Utilities Support Equipment Based Solid State Transformer (MUSE-SST) with 10 KV SiC MOSFETs for Grid Interconnection. In Proceedings of the 2018 9th IEEE International Symposium on Power Electronics for Distributed Generation Systems (PEDG), Charlotte, NC, USA, 25–28 June 2018; IEEE: Piscataway, NJ, USA, 2018; pp. 1–8.
41. Jianqiao, Z.; Jianwen, Z.; Xu, C.; Jiacheng, W.; Jiajie, Z. Family of Modular Multilevel Converter (MMC) Based Solid State Transformer (SST) Topologies for Hybrid AC/DC Distribution Grid Applications. In Proceedings of the 2018 IEEE International Power Electronics and Application Conference and Exposition (PEAC), Shenzhen, China, 4–7 November 2018; IEEE: Piscataway, NJ, USA, 2018; pp. 1–5.
42. Niyitegeka, G.; Harerimana, E.M.; Park, G.; Choi, J. Phase Shift Modulation and DC-Link's Voltage Balancing Control for a DAB DC-DC Converter. In Proceedings of the 2018 International Conference on Smart Grid (icSmartGrid), Nagasaki, Japan, 4–6 December 2018; IEEE: Piscataway, NJ, USA, 2018; pp. 70–75.
43. Agrawal, A.; Nalamati, C.S.; Gupta, R. Hybrid DC–AC Zonal Microgrid Enabled by Solid-State Transformer and Centralized ESD Integration. *IEEE Trans. Ind. Electron.* **2019**, *66*, 9097–9107. [CrossRef]
44. Pugliese, S.; Buticchi, G.; Mastromauro, R.A.; Andresen, M.; Liserre, M.; Stasi, S. Soft-Start Procedure for a Three-Stage Smart Transformer Based on Dual-Active Bridge and Cascaded H-Bridge Converters. *IEEE Trans. Power Electron.* **2020**, *35*, 11039–11052. [CrossRef]
45. Choi, H.-J.; Jung, J.-H. Practical Design of Dual Active Bridge Converter as Isolated Bi-Directional Power Interface for Solid State Transformer Applications. *J. Electr. Eng. Technol.* **2016**, *11*, 1265–1273. [CrossRef]
46. Lai, J.-S.; Lai, W.-H.; Moon, S.-R.; Zhang, L.; Maitra, A. A 15-KV Class Intelligent Universal Transformer for Utility Applications. In Proceedings of the 2016 IEEE Applied Power Electronics Conference and Exposition (APEC), Long Beach, CA, USA, 20–24 March 2016; IEEE: Piscataway, NJ, USA, 2016; pp. 1974–1981.
47. Wang, D.; Tian, J.; Mao, C.; Lu, J.; Duan, Y.; Qiu, J.; Cai, H. A 10-KV/400-V 500-KVA Electronic Power Transformer. *IEEE Trans. Ind. Electron.* **2016**, *63*, 6653–6663. [CrossRef]
48. Costa, L.F.; Buticchi, G.; Liserre, M. Quadruple Active Bridge DC-DC Converter as the Basic Cell of a Modular Smart Transformer. In Proceedings of the 2016 IEEE Applied Power Electronics Conference and Exposition (APEC), Long Beach, CA, USA, 20–24 March 2016; IEEE: Piscataway, NJ, USA, 2016; pp. 2449–2456.
49. Costa, L.F.; Buticchi, G.; Liserre, M. Quad-Active-Bridge DC–DC Converter as Cross-Link for Medium-Voltage Modular Inverters. *IEEE Trans. on Ind. Applicat.* **2017**, *53*, 1243–1253. [CrossRef]
50. Costa, L.F.; Hoffmann, F.; Buticchi, G.; Liserre, M. Comparative Analysis of Multiple Active Bridge Converters Configurations in Modular Smart Transformer. *IEEE Trans. Ind. Electron.* **2019**, *66*, 191–202. [CrossRef]
51. Shi, H.; Wen, H.; Hu, Y.; Yang, Y.; Wang, Y. Efficiency Optimization of DC Solid-State Transformer for Photovoltaic Power Systems. *IEEE Trans. Ind. Electron.* **2020**, *67*, 3583–3595. [CrossRef]
52. Lee, J.; Roh, J.; Kim, M.Y.; Baek, S.-H.; Kim, S.; Lee, S.-H. A Novel Solid-State Transformer with Loosely Coupled Resonant Dual-Active-Bridge Converters. *IEEE Trans. Ind. Appl.* **2022**, *58*, 709–719. [CrossRef]

53. Parreiras, T.M.; Machado, A.P.; Amaral, F.V.; Lobato, G.C.; Brito, J.A.S.; Filho, B.C. Forward Dual-Active-Bridge Solid-State Transformer for a SiC-Based Cascaded Multilevel Converter Cell in Solar Applications. *IEEE Trans. Ind. Appl.* **2018**, *54*, 6353–6363. [CrossRef]
54. Amaral, F.V.; Parreiras, T.M.; Lobato, G.C.; Machado, A.A.P.; Pires, I.A.; de Jesus Cardoso Filho, B. Operation of a Grid-Tied Cascaded Multilevel Converter Based on a Forward Solid-State Transformer Under Unbalanced PV Power Generation. *IEEE Trans. Ind. Appl.* **2018**, *54*, 5493–5503. [CrossRef]
55. Sharma, R.; Sharma, S.K. Solar Photovoltaic Supply System Integrated with Solid State Transformer. In Proceedings of the 2021 IEEE 4th International Conference on Computing, Power, and Communication Technologies (GUCON), Kuala Lumpur, Malaysia, 24–26 September 2021; pp. 1–6.
56. Smith, C.; Haque, M.E. Design and Implementation of a Smart Solid-State Transformer Based Power Converter for Solar PV System. In Proceedings of the 2020 IEEE Industry Applications Society Annual Meeting, Detroit, MI, USA, 10–16 October 2020; pp. 1–8.
57. Voltage Transducer LV 25-P—LEM. Available online: https://www.lem.com/sites/default/files/products_datasheets/lv_25-p.pdf (accessed on 23 November 2022).
58. Ourahou, M.; Ayrir, W.; EL Hassouni, B.; Haddi, A. Review on Smart Grid Control and Reliability in Presence of Renewable Energies: Challenges and Prospects. *Math. Comput. Simul.* **2020**, *167*, 19–31. [CrossRef]
59. Huang, P.; Xu, T.; Sun, Y. A Genetic Algorithm Based Dynamic Pricing for Improving Bi-Directional Interactions with Reduced Power Imbalance. *Energy Build.* **2019**, *199*, 275–286. [CrossRef]
60. Anurag, A.; Acharya, S.; Prabowo, Y.; Gohil, G.; Bhattacharya, S. Design Considerations and Development of an Innovative Gate Driver for Medium-Voltage Power Devices with High $ Dv/Dt$. *IEEE Trans. Power Electron.* **2018**, *34*, 5256–5267. [CrossRef]